Controlling filamentous cyanobacterial blooms requires adaptive, weather-informed strategy

Supplementary Material

Jiao Fang[a,b] Ming Su[a,e,*] Yande Li[c] Yuying Gui[a,d] Yufan Ai[a,e] Ogalo Joseph[a,e]
Tengxin Cao[a,e] Shilong He[b] Min Yang[a,e,*]

[a] Key Laboratory of Environmental Aquatic Chemistry, State Key Laboratory of Regional Environment and Sustainability, Research Center for Eco-Environmental Sciences, Chinese Academy of Sciences, Beijing 100085, China.

[b] School of Environment and Spatial Informatics, China University of Mining and Technology, Xuzhou 221116, China.

[c] Management Station of Shuangxikou Reservoir, Reservoir Management Service Center of Yuyao, Ningbo 315423, China.

[d] College of Environmental Science and Engineering, Ocean University of China, Qingdao 266100, China.

[e] University of Chinese Academy of Sciences, Beijing 100049, China.

[*] Corresponding to: Ming Su (mingsu@rcees.ac.cn), Min Yang (yangmin@rcees.ac.cn)

Figures and/or tables are provided below as the supplementary evidences to the main text.

Comparative analysis of algal mitigation strategies

Method	Genera	Advantages	Disadvantages	Reference
Copper sulfate	*Microcystis*	Rapid efficacy	Copper ion residuals; Disrupts microbial diversity	(Liu et al., 2023)
Copper sulfate	*Pseudokirchneriella*	Easy operation	High resistance	(Tsai, 2016)
Solid sodium percarbonate	*Pseudanabaena*	Less impact on microbial diversity	Differentiated response	(Xu et al., 2021)
Ultrasound	*Microcystis*	No chemical additives; Disruption of gas vesicles	High energy demand; Ineffective against small algae	(Kong et al., 2019)
Ultrasound	*Hydrodictyon*	Fragments trichomes	Limited effectiveness	(Lee et al., 2014)
Aeration/mixing	*Microcystis*	Inhibition of surface aggregation	Limited effectiveness in emergency situation	(He et al., 2024)
Flocculation	*Microcystis, Pseudanabaena*	High efficiency	Aluminum residuals; Introduction of additional substances; Pre-treatment requirement	(Li and Pan, 2015; Xu et al., 2024)
Sediment Resuspension	*Pseudanabaena*	Spectral targeting; Eco-sustainability; Cost-effectiveness	Threshold limitation; Turbidity increase; Not applicable under sediment contamination	this study; (Fang et al., 2024; Su et al., 2025)

Table S1: Comparative analysis of algal mitigation strategies: Conventional versus SR-based approaches.

Seasonal distribution of filamentous cyanobacteria density range across 40 reservoirs

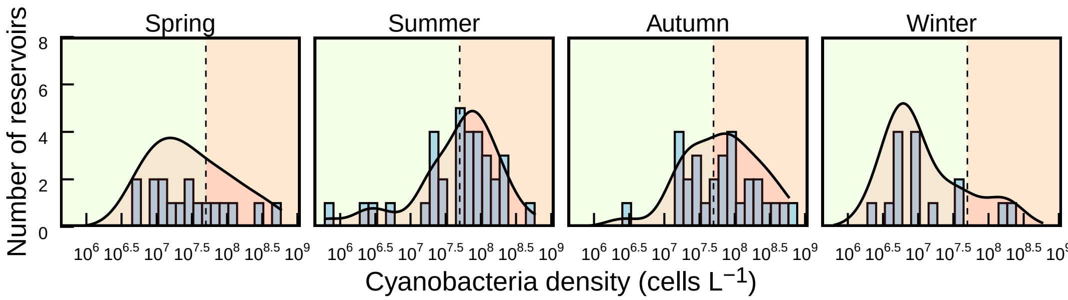

Fig. S1: Seasonal distribution of filamentous cyanobacteria density range across 40 reservoirs. Spring through Winter histograms showing reservoir counts (n = 40) binned by cyanobacteria density intervals (cells L^{-1}). Vertical dashed lines indicate critical risk thresholds: green (low risk: < 5 × 10^7 cells L^{-1}) and orange (moderate risk: > 5 × 10^7 cells L^{-1}).

Distribution of nutrients concentration range across 40 reservoirs

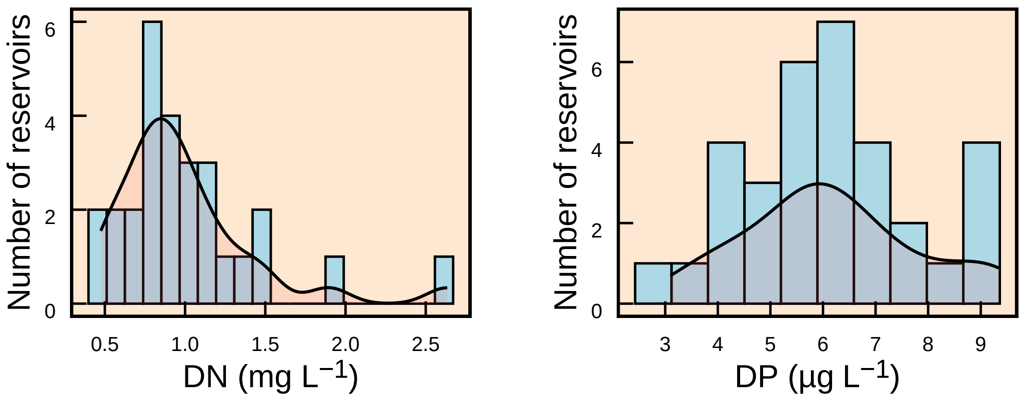

Fig. S2: Distribution of nutrients concentration range across 40 reservoirs. Histograms showing reservoir counts (n = 40) binned by dissolved nitrogen (DN) and dissolved phosphorus (DP) intervals.

Temporal dynamics and statistical distribution of underwater light intensity across experimental treatments

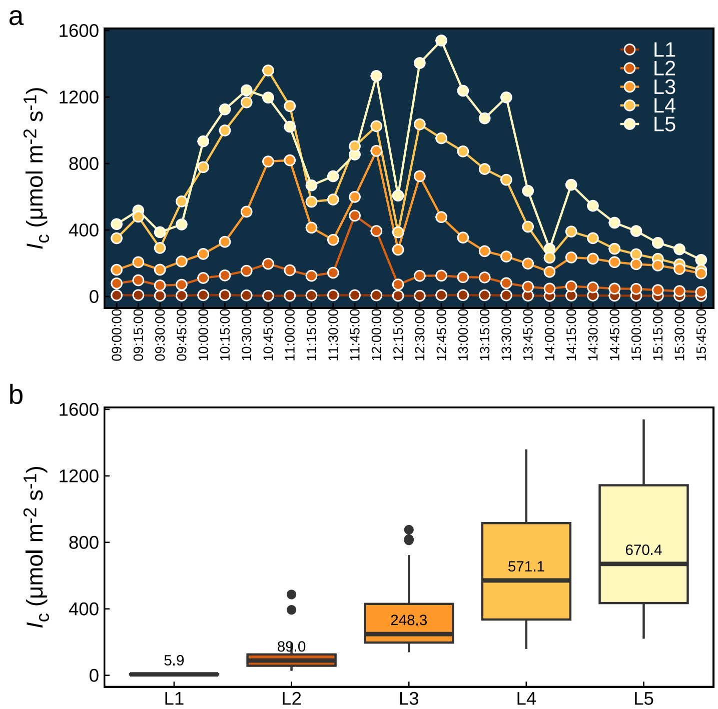

Fig. S3: Temporal dynamics and statistical distribution of underwater light intensity ($I_{c(0.05m)}$) across experimental shading treatments. a, High-resolution measurements of underwater light intensity (μmol m^{-2} s^{-1}) at 0.05 m depth under graduated shading treatments (0 – 98% surface coverage), recorded at 15-min intervals (09:00 – 16:00) during Day 1 of sediment resuspension (SR) deployment. b, Boxplot analysis of light regimes by treatment, showing statistically distinct reductions in $I_{c(0.05m)}$ relative to unshaded controls.

Temporal dynamics of dissolved nitrogen concentration across experimental treatments

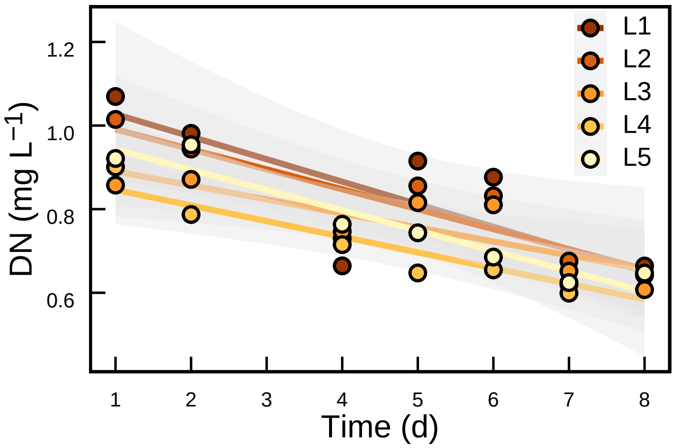

Fig. S4: Temporal dynamics of dissolved nitrogen concentration across experimental treatments

Seasonal variations in mixed layer depth across 40 drinking water reservoirs

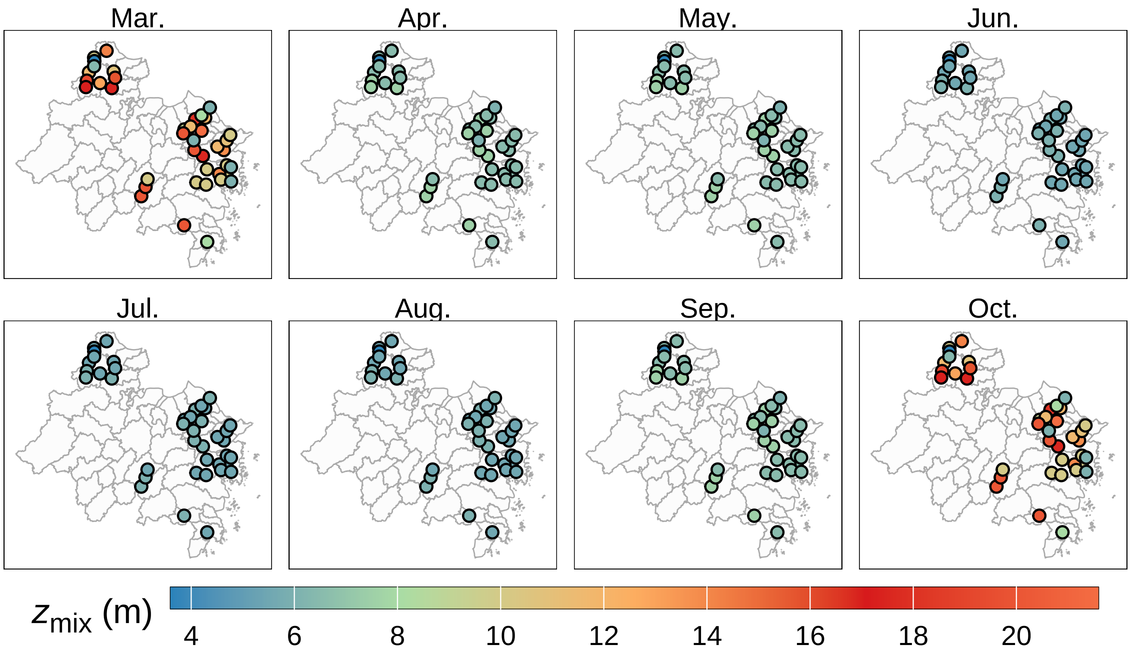

Fig. S5: Seasonal variations in mixed layer depth (z_{mix}) across 40 drinking water reservoirs.

Seasonal variations in underwater light available across 40 drinking water reservoirs

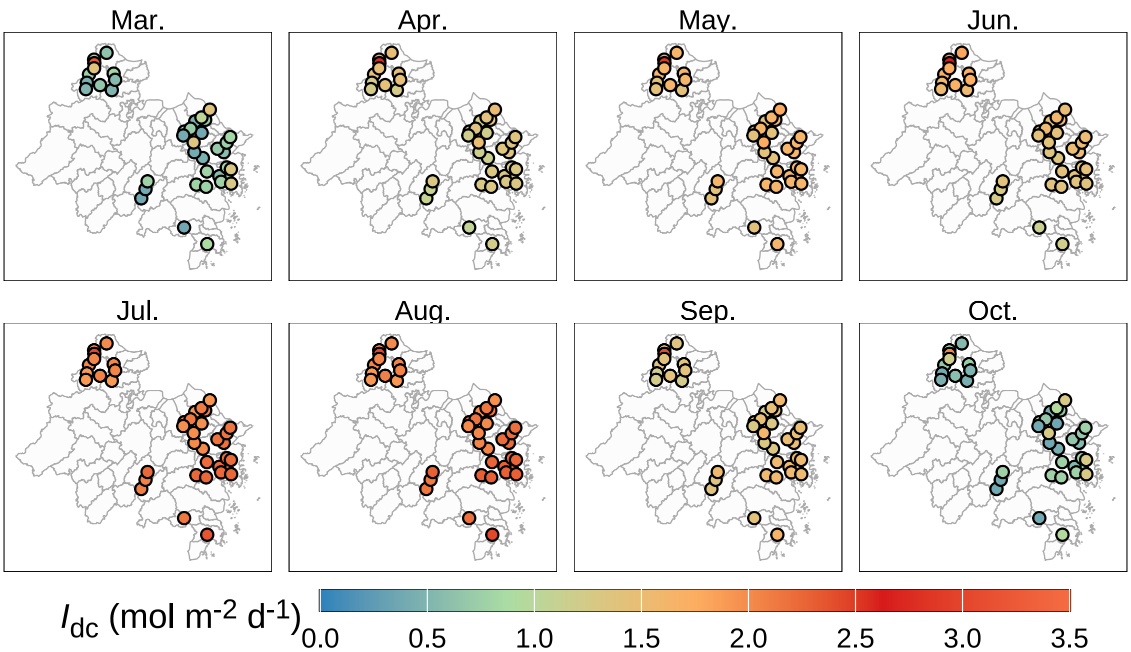

Fig. S6: Seasonal variations in underwater light available (I_{dc}) across 40 drinking water reservoirs.

Seasonal variations in water temperature across 40 drinking water reservoirs

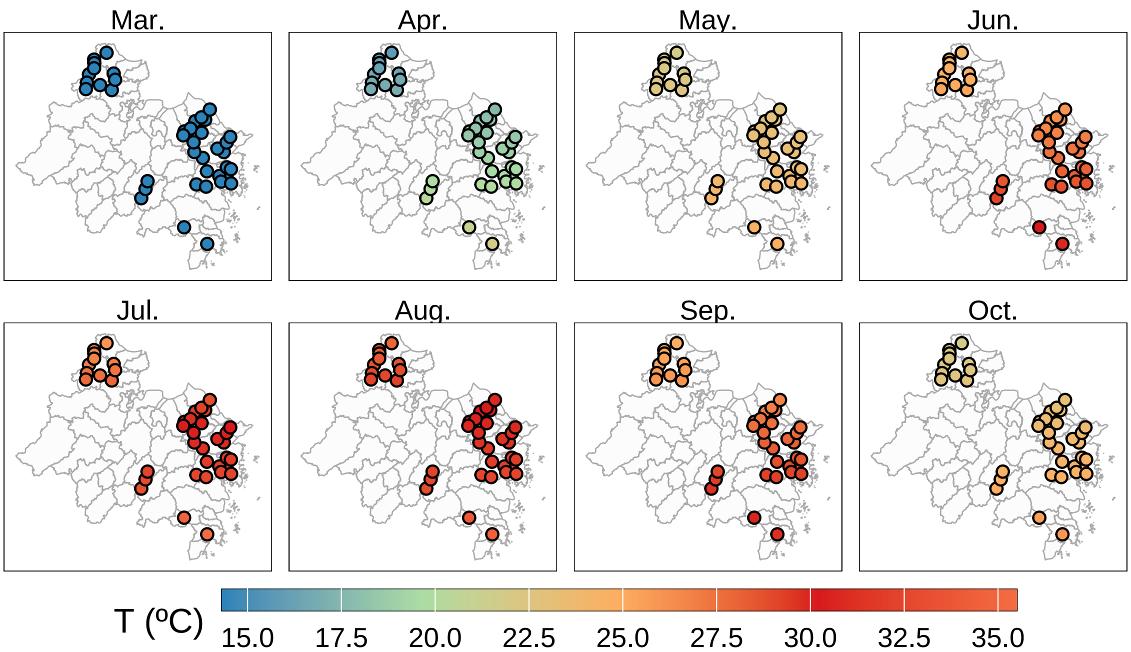

Fig. S7: Seasonal variations in water temperature (T) across 40 drinking water reservoirs.

Seasonal dynamics of predicted filamentous cyanobacteria density and environmental drivers across 40 reservoirs

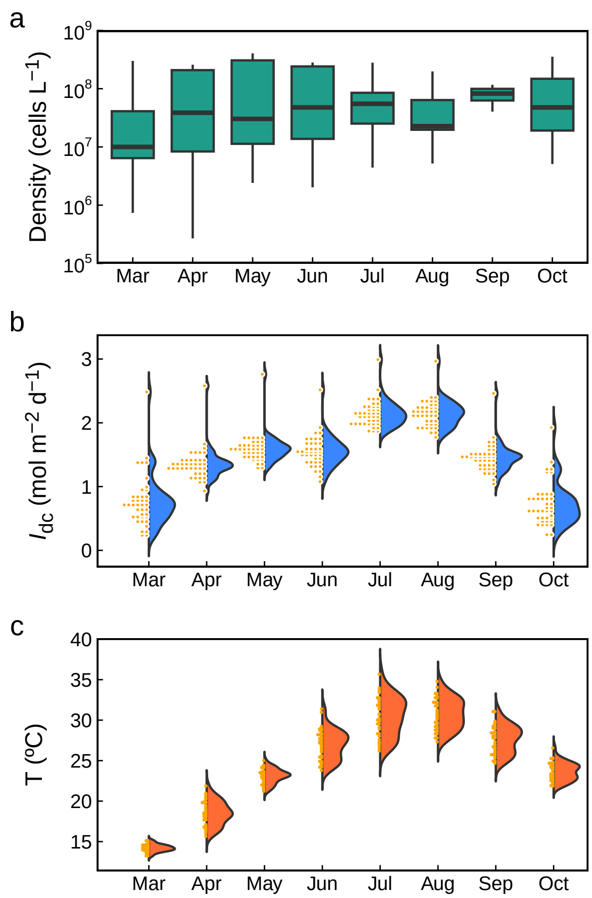

Fig. S8: Seasonal dynamics of predicted filamentous cyanobacteria density and environmental drivers across 40 reservoirs. a, Monthly distributions of predicted filamentous cyanobacteria cell densities (cells L^{-1}) from March to October. **b,** Corresponding underwater light available (I_{dc}). **c,** Corresponding underwater temperature (T).

Monthly distribution of predicted filamentous cyanobacteria density risk range across 40 reservoirs

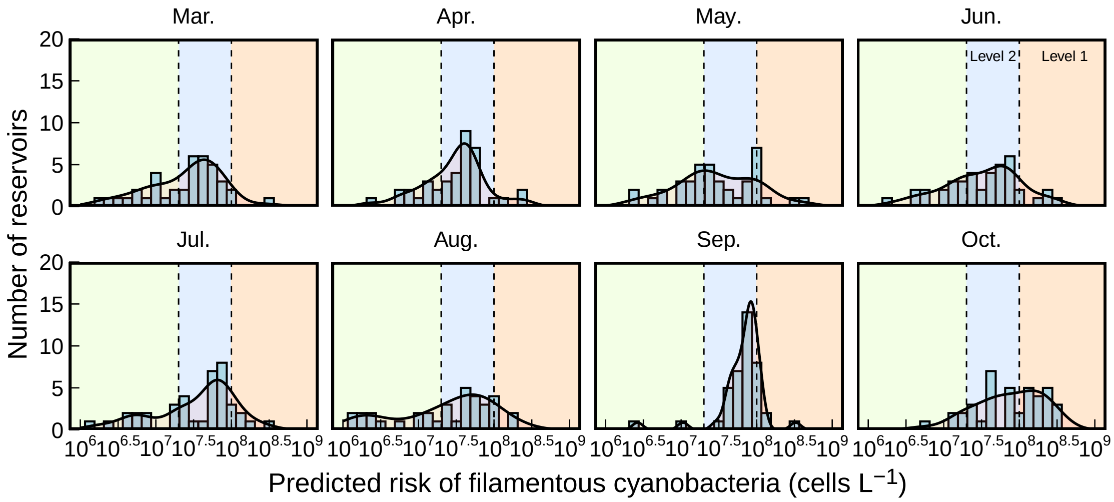

Fig. S9: Monthly distribution of predicted filamentous cyanobacteria density risk range across 40 reservoirs. March through October histograms showing reservoir counts (n = 40) binned by predicted algal density intervals (cells L^{-1}). Vertical dashed lines indicate two risk thresholds: Risk Level 1 (RL_1): 1×10^8 cell L^{-1} and Risk Level 2 (RL_2): 2×10^7 cell L^{-1}. The diferent colors represent different risk levels: green (low risk: < RL_2), blue (moderate risk: RL_2 to RL_1) and orange (high risk: > RL_1).

Seasonal control rates of filamentous cyanobacteria bloom mitigation across 40 reservoirs

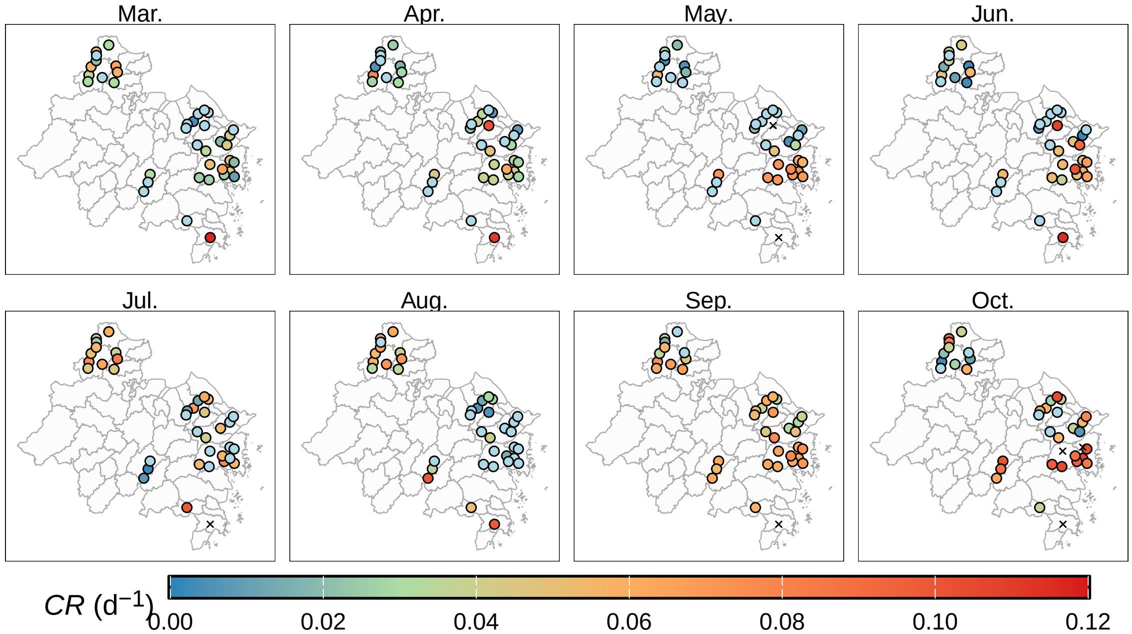

Fig. S10: Seasonal control rates (*CR*) of filamentous cyanobacteria bloom mitigation across 40 reservoirs. Monthly success rates for reducing predicted filamentous cyanobacteria densities from initial bloom conditions to target Risk Level 2 (RL_2: 2×10^7 cells L^{-1}) within 10 days.

Monthly effectiveness of sediment resuspension for controlling filamentous cyanobacteria blooms across 40 reservoirs

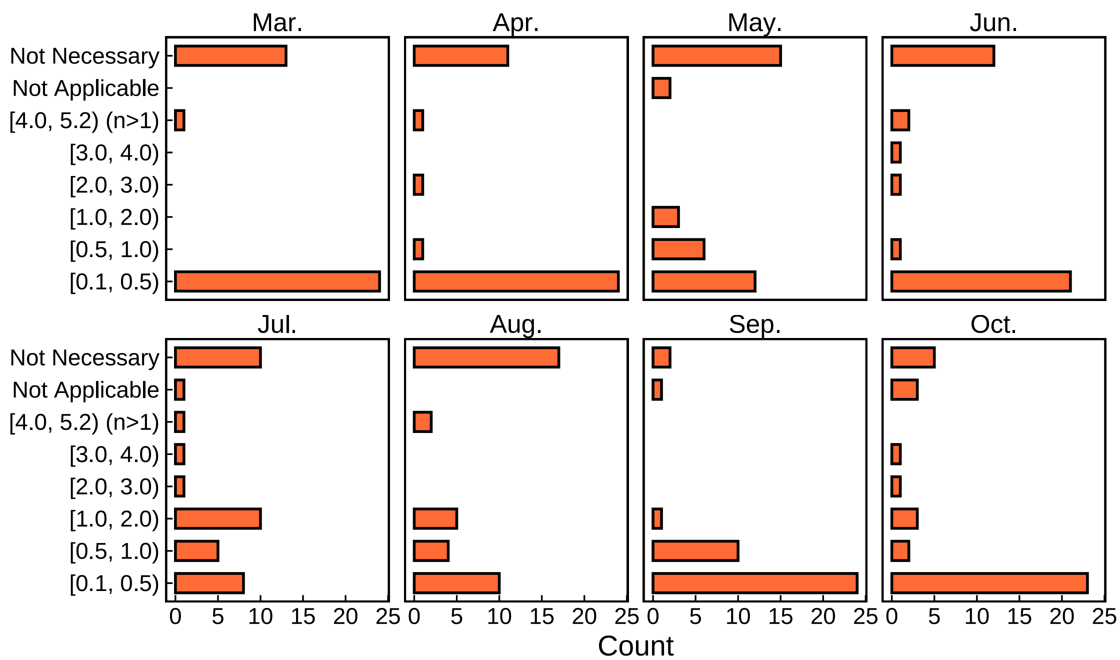

Fig. S11: Monthly effectiveness of sediment resuspension for controlling filamentous cyanobacteria blooms across 40 reservoirs. Monthly plots showing how many reservoirs successfully reduced algal levels below Risk Level 2 (RL_2: 2×10^7 cells L^{-1}) within N (N = 10) days using different sediment resuspension strategies. Each panel represents a month from March to October. The x-axis shows eight sediment resuspension conditions combining two different frequencies ($n = 1$ and $n > 1$) and six sediment concentration ranges.

Temporal dynamics of underwater light available across bloom stage in S Reservoir

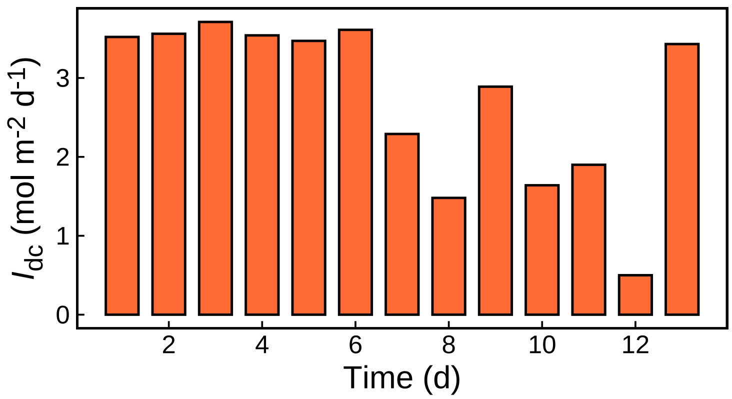

Fig. S12: Temporal dynamics of underwater light available (I_{dc}) across bloom stage in S Reservoir.

Workflow for determining the optimal sediment resuspension (SR) operating conditions

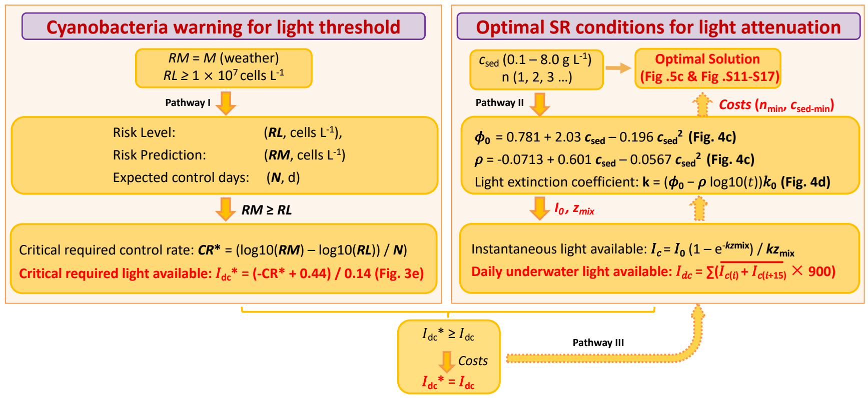

Fig. S13: Workflow for determining the optimal sediment resuspension (SR) operating conditions. It was structured into three pathways: (I) The critical control rate (CR^*) and light-threshold ($I^*_{\rm dc}$) determination. CR^* was first determined based upon the bloom risk predictions (RM) across 40 reservoirs over different months, and the $I^*_{\rm dc}$ is derived from the filamentous cyanobacteria control target (Risk Level RL and Expected control days N); (II) SR-driven optical attenuation estimation, which calculates achievable $I_{\rm dc}$ from extinction coefficient responses (k) under different sediment concentrations ($c_{\rm sed}$) and resuspension frequencies (n); (III) Cost-constrained optimization, which identifies the most efficient SR regime by sequentially meeting the criteria ($I_{\rm dc} = I^*_{\rm dc}$, $n_{\rm min}$, $c_{\rm sed(min)}$).

Dynamics of nutrients concentration before and during SR in S Reservoir

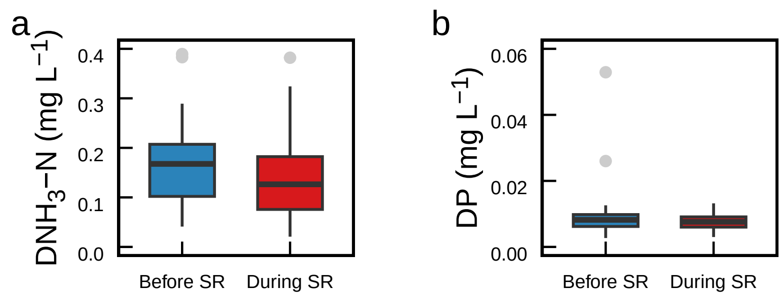

Fig. S14: Dynamics of dissolved ammonia nitrogen and dissolved phosphorus before and during SR in S Reservoir

Field applications in five drinking water reservoirs

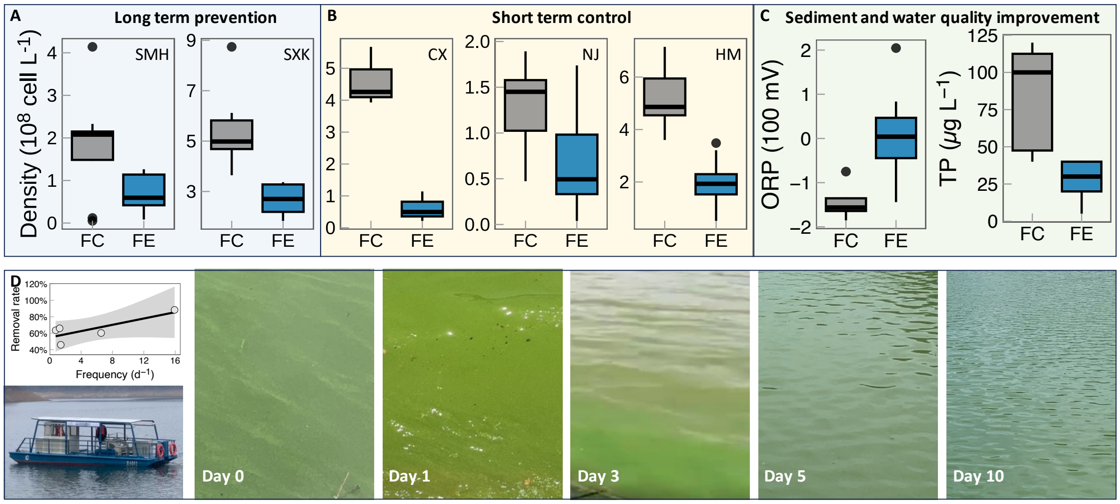

Fig. S15: The comparison of observed total phytoplankton cell densities between sites with Sediment Resuspension (SR) operations (FE) and those without (FC) was conducted across five drinking water reservoirs. Long-term SR technology was implemented in SMH and SXK Reservoirs to evaluate its effectiveness in preventing cyanobacterial growth (A), while the CX, NJ, and HM Reservoirs underwent short-term evaluation for cyanobacterial bloom control (B). Panel C illustrates the comparison of Oxidation-Reduction Potential (ORP) of reservoir sediment and total phosphorus concentration of reservoir water, assessing the effect of long-term SR on sediment and water quality. Furthermore, panel D depicts the relationship between cell removal rate and SR working intensity, accompanied by several images that document the changes in the water surface of the CX Reservoir following SR operations from day 0 to day 10. Notably, a severe *Microcystis* bloom in the CX Reservoir provided a vivid visual representation of the changes in the water bodies.

Optimal SR flux for control of filamentous cyanobacterial blooms under various meteorological conditions, bloom intensities and mixed layer

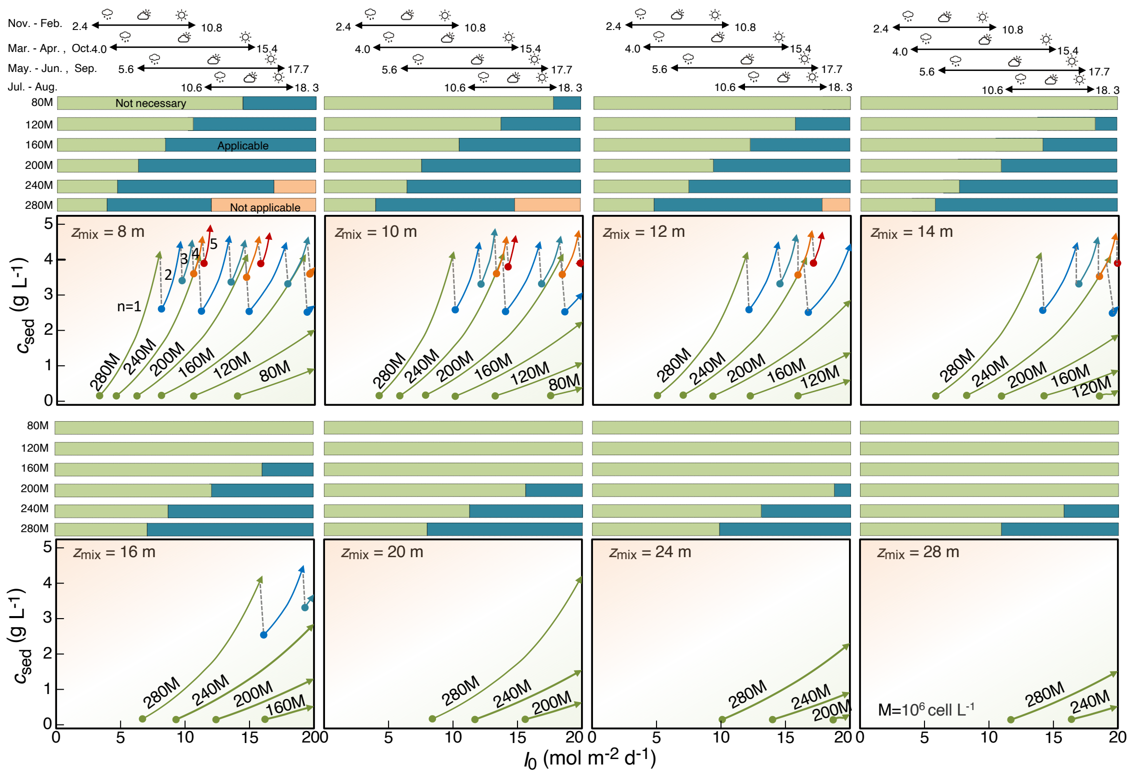

Fig. S16: Optimal SR flux for control of filamentous cyanobacterial blooms under various meteorological conditions (daily surface light intensity, I_0, 0 - 20 mol m^{-2} d^{-1}), bloom intensities (0.8 - 2.8 × 10^8 cells L^{-1}) and mixed layer depths (8 - 28 m).

Sketch of weather-based implementation of underwater light regulation

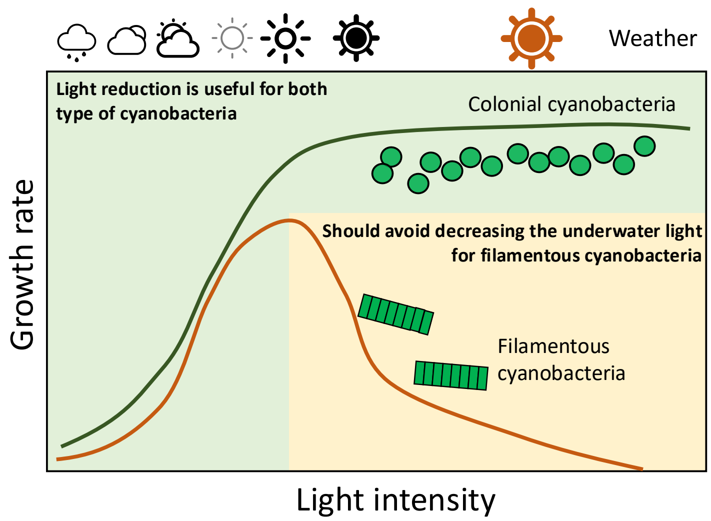

Fig. S17: Sketch of weather-based implementation of underwater light regulation.

Light modulation efficacy for controlling filamentous cyanobacteria blooms with z_{mix} of 6 m under varying solar regimes

No. 1 Light modulation efficacy under initial predicted density of 80 M under z_{mix} of 6 m

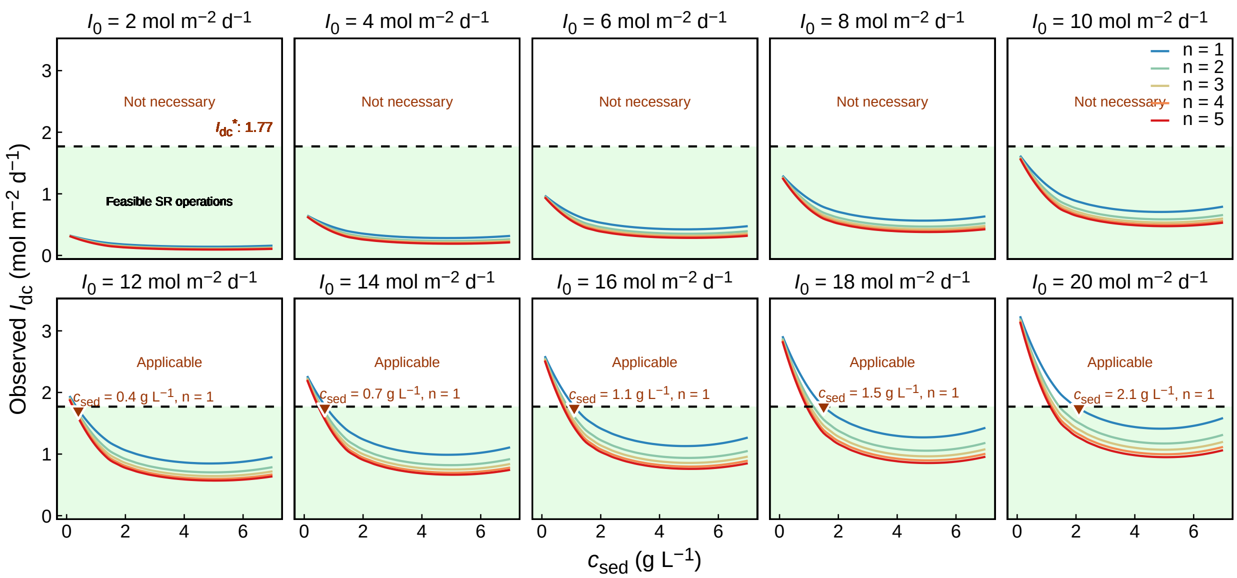

Fig. S18: Light modulation efficacy under initial predicted density of 80 M under z_{mix} of 6 m. Dynamics of underwater irradiance (I_0, 2 - 20 µmol m^{-2} d^{-1} etc,.) across sediment resuspension (SR) conditions (x-axis: sediment concentration 0.1 - 8.0 g L^{-1}; color: resuspension frequency 1 - 5 cycles d^{-1}), faceted by incident solar radiation quartiles. Horizontal dashed lines indicate critical light thresholds required to suppress blooms from initial predicted density of 0.8 × 10^{8} cells L^{-1} to Risk Level 2 (RL_2: 2 × 10^{7} cells L^{-1}) within N (N = 10) days. Brown points denote optimal SR parameters balancing algal control and operational cost (minimal sediment loading).

No. 2 Light modulation efficacy under initial predicted density of 120 M under z_{mix} of 6 m

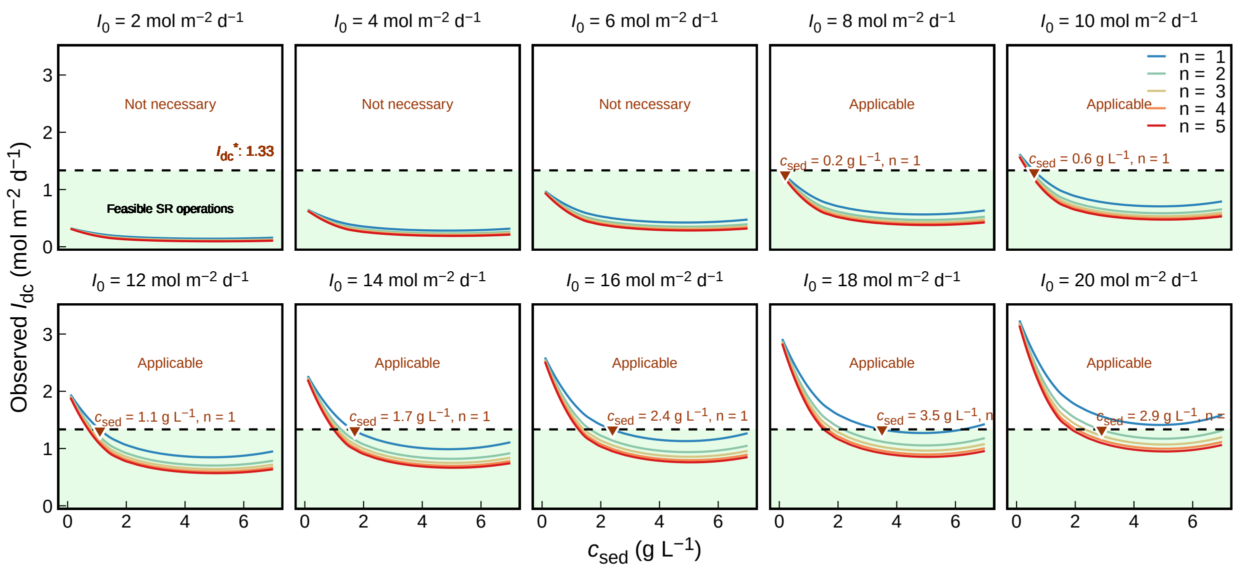

Fig. S19: Light modulation efficacy under initial predicted density of 120 M under z_{mix} of 6 m. Dynamics of underwater irradiance (I_0, 2 - 20 µmol m^{-2} d^{-1} etc,.) across sediment resuspension (SR) conditions (x-axis: sediment concentration 0.1 - 8.0 g L^{-1}; color: resuspension frequency 1 - 5 cycles d^{-1}), faceted by incident solar radiation quartiles. Horizontal dashed lines indicate critical light thresholds required to suppress blooms from initial predicted density of 1.2×10^8 cells L^{-1} to Risk Level 2 (RL_2: 2×10^7 cells L^{-1}) within N (N = 10) days. Brown points denote optimal SR parameters balancing algal control and operational cost (minimal sediment loading).

No. 3 Light modulation efficacy under initial predicted density of 160 M under z_{mix} of 6 m

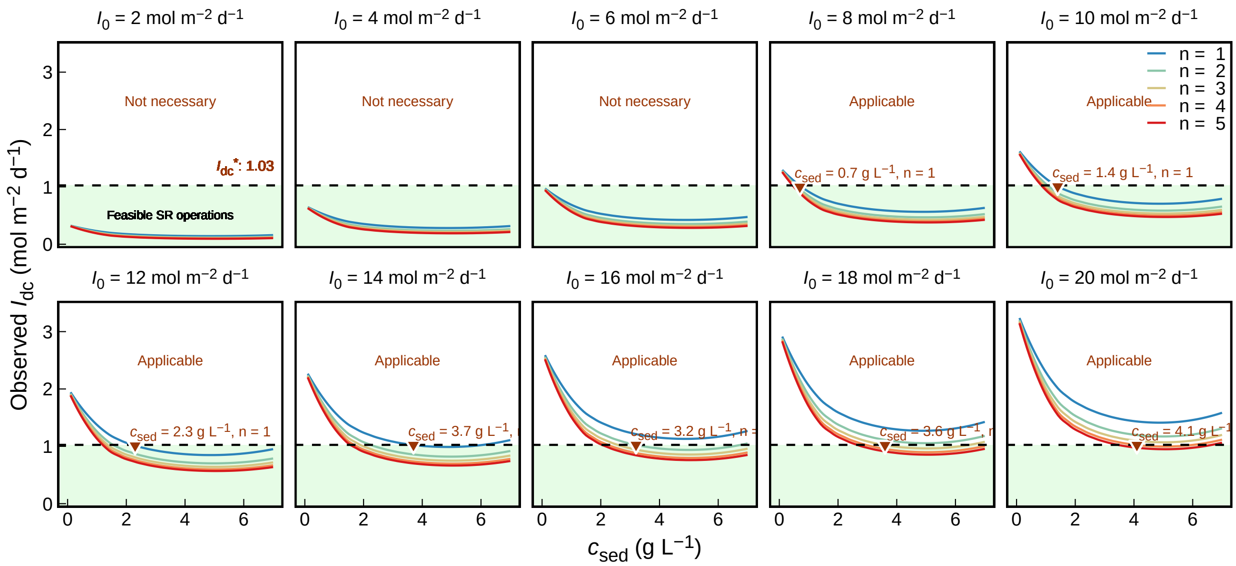

Fig. S20: Light modulation efficacy under initial predicted density of 160 M under z_{mix} of 6 m. Dynamics of underwater irradiance (I_0, 2 - 20 μmol m^{-2} d^{-1} etc,.) across sediment resuspension (SR) conditions (x-axis: sediment concentration 0.1 - 8.0 g L^{-1}; color: resuspension frequency 1 - 5 cycles d^{-1}), faceted by incident solar radiation quartiles. Horizontal dashed lines indicate critical light thresholds required to suppress blooms from initial predicted density of 1.6 × 10^8 cells L^{-1} to Risk Level 2 (RL_2: 2 × 10^7 cells L^{-1}) within N (N = 10) days. Brown points denote optimal SR parameters balancing algal control and operational cost (minimal sediment loading).

No. 4 Light modulation efficacy under initial predicted density of 200 M under z_{mix} of 6 m

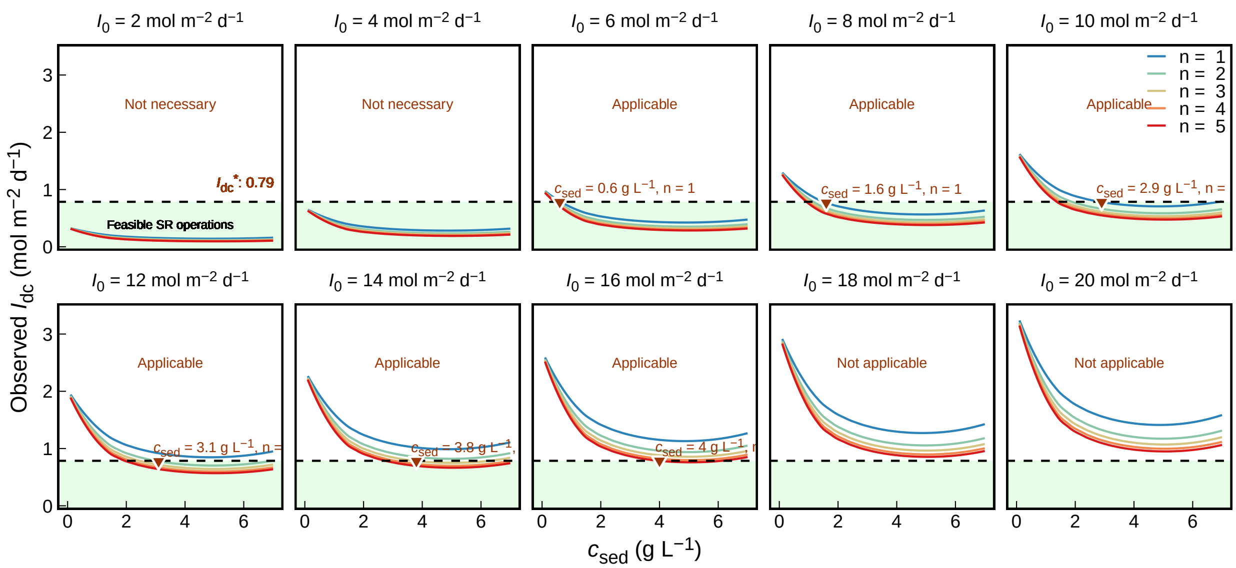

Fig. S21: Light modulation efficacy under initial predicted density of 200 M under z_{mix} of 6 m. Dynamics of underwater irradiance (I_0, 2 - 20 µmol m^{-2} d^{-1} etc,.) across sediment resuspension (SR) conditions (x-axis: sediment concentration 0.1 - 8.0 g L^{-1}; color: resuspension frequency 1 - 5 cycles d^{-1}), faceted by incident solar radiation quartiles. Horizontal dashed lines indicate critical light thresholds required to suppress blooms from initial predicted density of 2.0×10^8 cells L^{-1} to Risk Level 2 (RL_2: 2×10^7 cells L^{-1}) within N (N = 10) days. Brown points denote optimal SR parameters balancing algal control and operational cost (minimal sediment loading).

No. 5 Light modulation efficacy under initial predicted density of 240 M under z_{mix} of 6 m

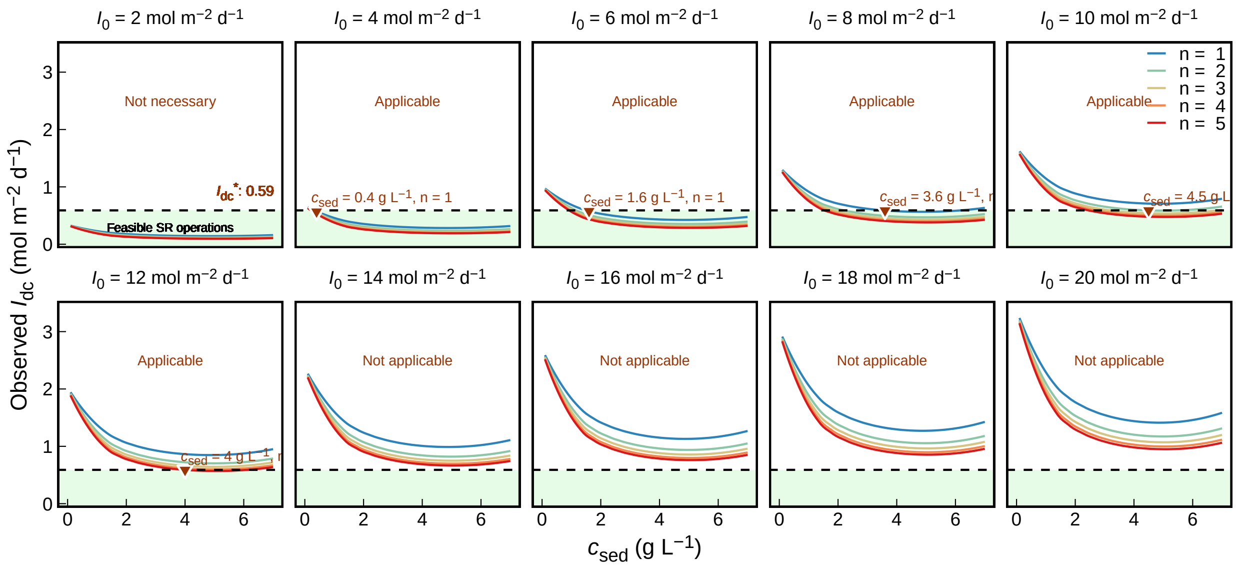

Fig. S22: Light modulation efficacy under initial predicted density of 240 M under z_{mix} of 6 m. Dynamics of underwater irradiance (I_0, 2 - 20 μmol m^{-2} d^{-1} etc,.) across sediment resuspension (SR) conditions (x-axis: sediment concentration 0.1 - 8.0 g L^{-1}; color: resuspension frequency 1 - 5 cycles d^{-1}), faceted by incident solar radiation quartiles. Horizontal dashed lines indicate critical light thresholds required to suppress blooms from initial predicted density of 2.4 × 10^8 cells L^{-1} to Risk Level 2 (RL_2: 2 × 10^7 cells L^{-1}) within N (N = 10) days. Brown points denote optimal SR parameters balancing algal control and operational cost (minimal sediment loading).

No. 6 Light modulation efficacy under initial predicted density of 280 M under z_{mix} of 6 m

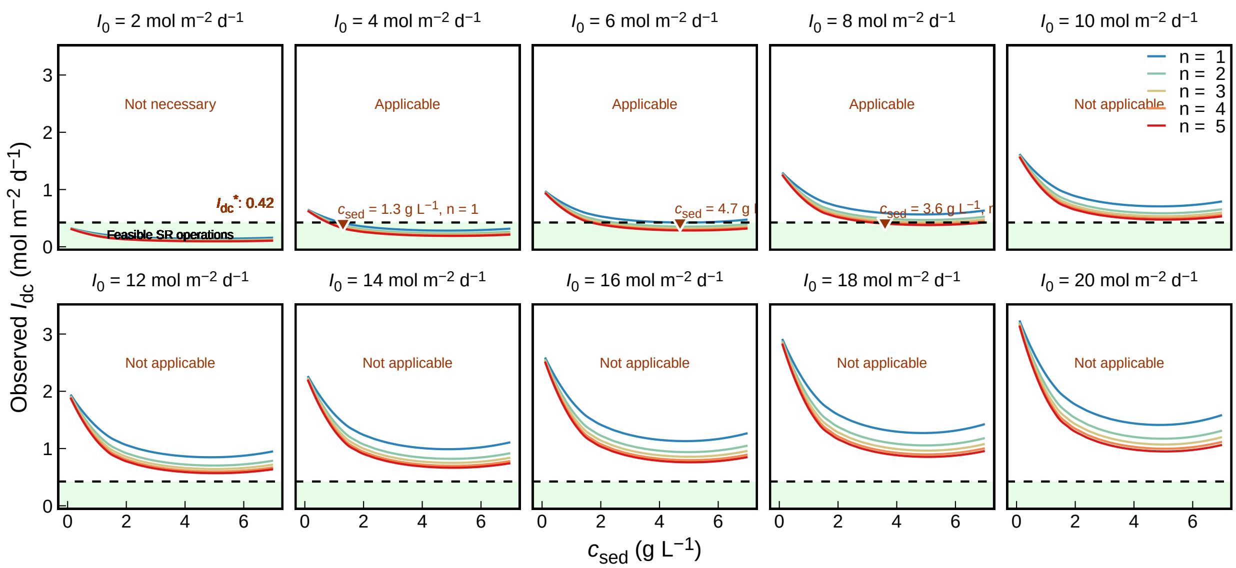

Fig. S23: Light modulation efficacy under initial predicted density of 280 M under z_{mix} of 6 m. Dynamics of underwater irradiance (I_0, 2 - 20 μmol m^{-2} d^{-1} etc,.) across sediment resuspension (SR) conditions (x-axis: sediment concentration 0.1 - 8.0 g L^{-1}; color: resuspension frequency 1 - 5 cycles d^{-1}), faceted by incident solar radiation quartiles. Horizontal dashed lines indicate critical light thresholds required to suppress blooms from initial predicted density of 2.8 × 10^8 cells L^{-1} to Risk Level 2 (RL_2: 2 × 10^7 cells L^{-1}) within N (N = 10) days. Brown points denote optimal SR parameters balancing algal control and operational cost (minimal sediment loading).

Observed variations in *Pseudanabaena* abundance across different light conditions

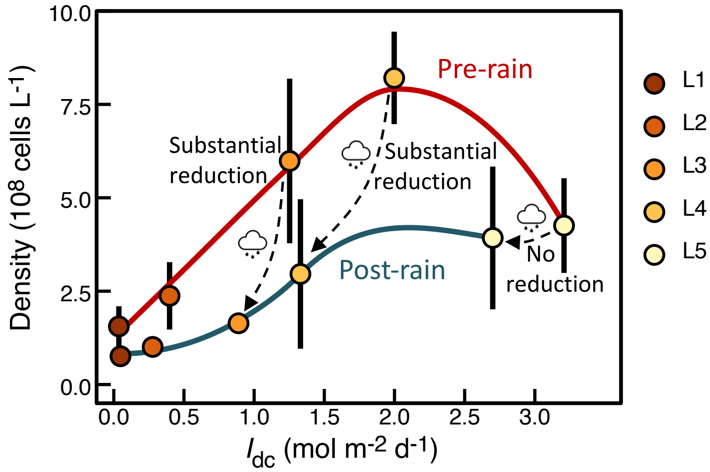

Fig. S24: A rainfall event reveals how ambient light regulates shading efficacy against filamentous cyanobacteria (*Pseudanabaena*) Differential impacts of identical shading treatments (L1–L5) on *Pseudanabaena* biomass during high-light pre-rain (S1) and low-light post-rain (S3) periods.

Growth responses of Microcystis* and filamentous cyanobacteria to light intensity

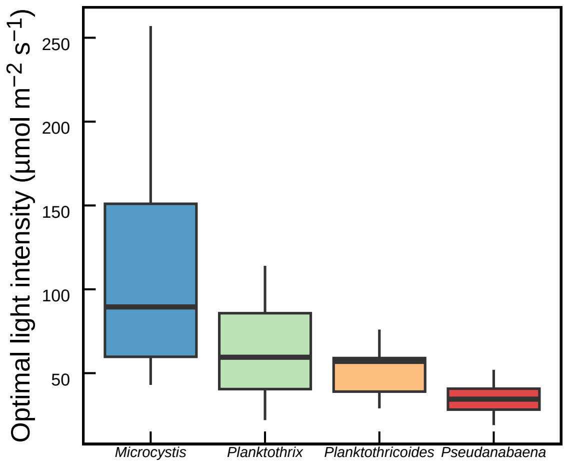

Fig. S25: Growth responses of *Microcystis* and filamentous cyanobacteria to light intensity, based on a synthesis of experimental studies.

Optimal sediment resuspension strategies for filamentous cyanobacteria control across seasonal 40 reservoir systems

No. 1 BX Reservoir

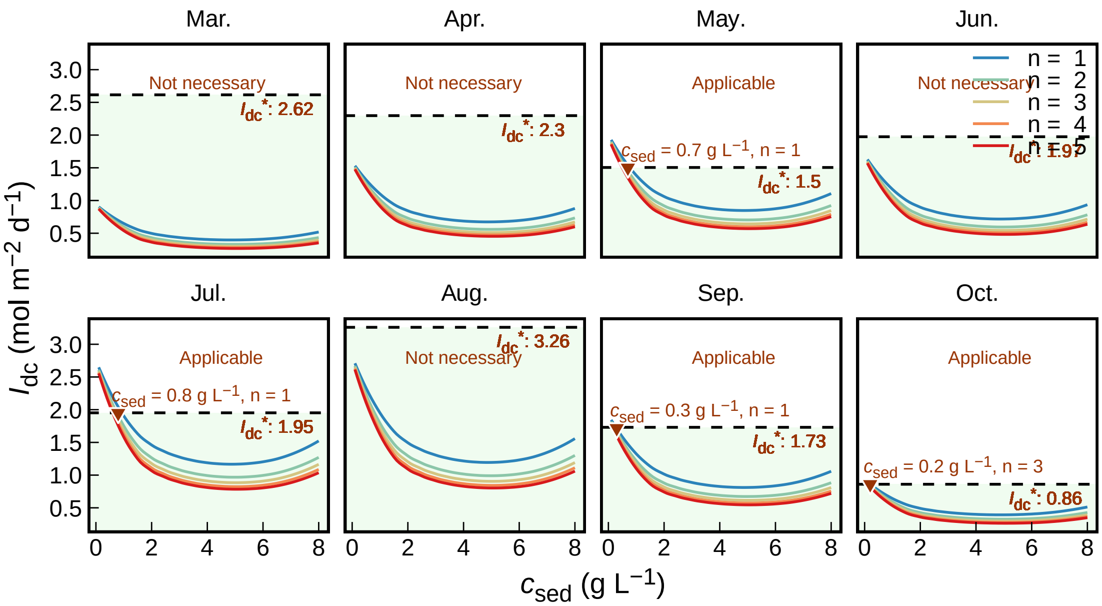

Fig. S26: Underwater light availability (y-axis) under varying sediment resuspension conditions (x-axis: sediment concentration, c_{sed}; color: resuspension frequency, n) in BX reservoir (March - October). Horizontal dashed lines indicate month-specific critical light thresholds (I_{dc}) required to suppress algal biomass to Risk Level 2 (RL_2: 2×10^7 cells L^{-1}) within N (N = 10) days. Conditions where resuspension-induced light attenuation falls below thresholds (points beneath dashed lines) represent effective algal control scenarios (green aera). Brown points identify optimal operational conditions - meeting critical light requirements while minimizing resuspension frequency, thereby balancing ecological efficacy with operational sustainability. Shaded regions highlight 95% confidence intervals for threshold responses.

No. 2 CAG Reservoir

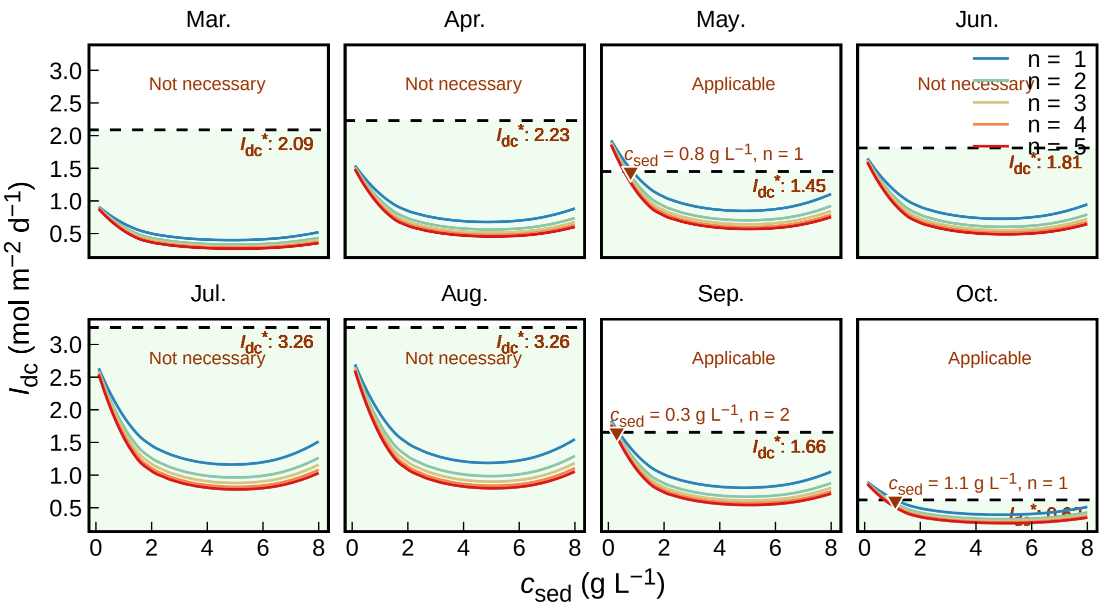

Fig. S27: Underwater light availability under varying sediment resuspension conditions in CAG reservoir (March - October).

No. 3 CT Reservoir

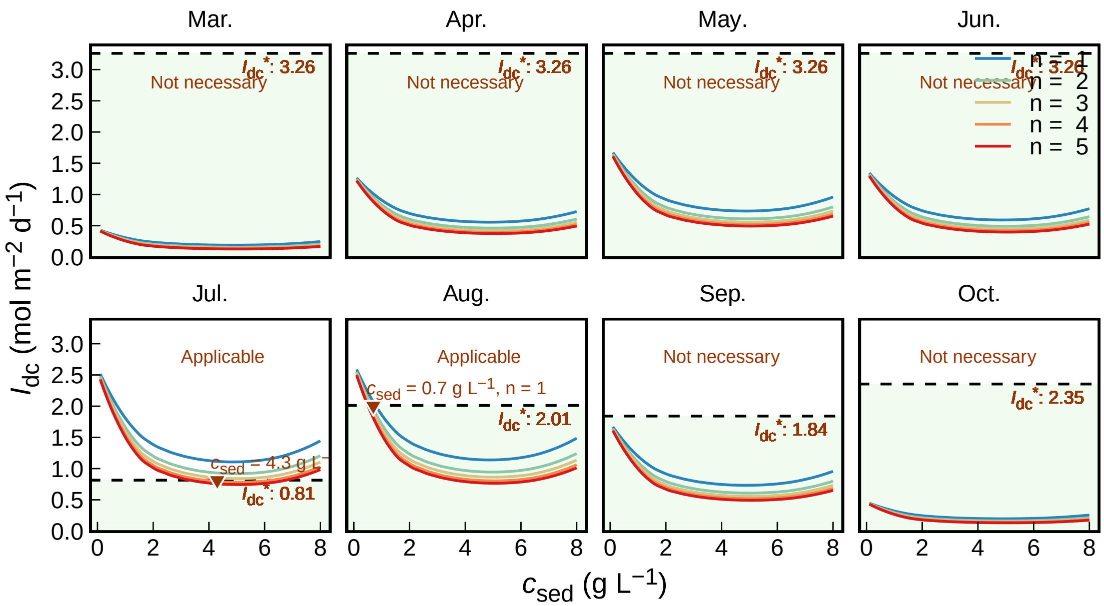

Fig. S28: Underwater light availability under varying sediment resuspension conditions in CT reservoir (March - October).

No. 4 DH Reservoir

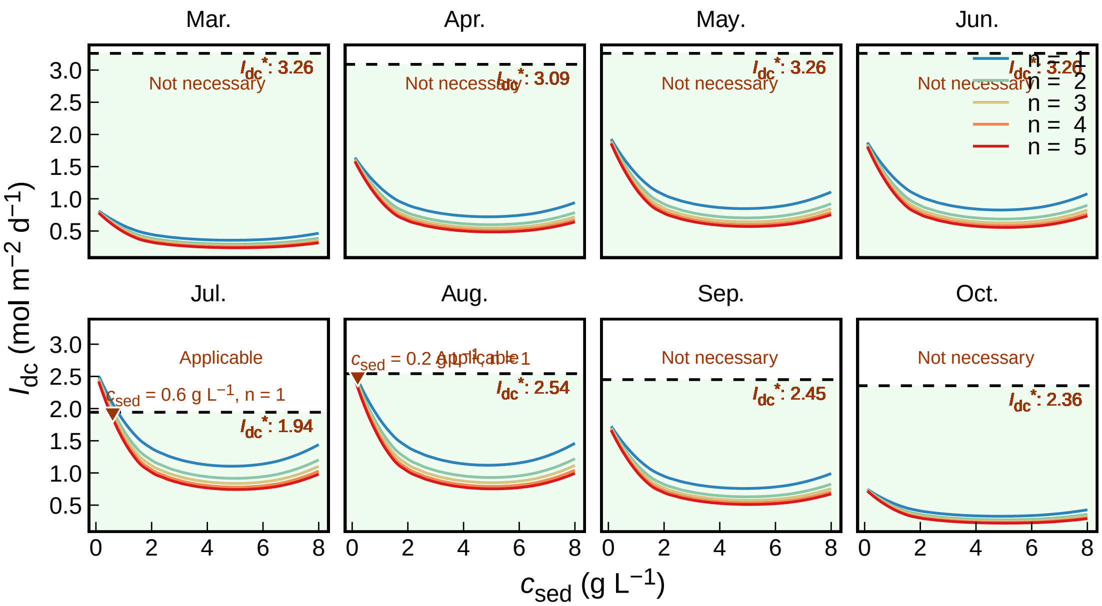

Fig. S29: Underwater light availability under varying sediment resuspension conditions in DH reservoir (March - October).

No. 5 DHK Reservoir

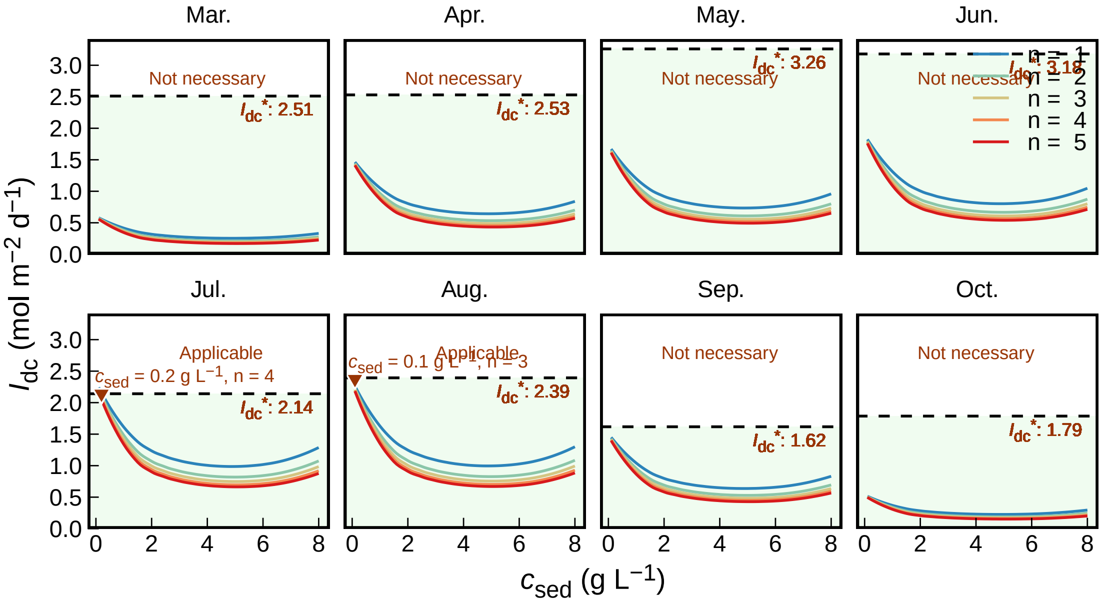

Fig. S30: Underwater light availability under varying sediment resuspension conditions in DHK reservoir (March - October).

No. 6 DTG Reservoir

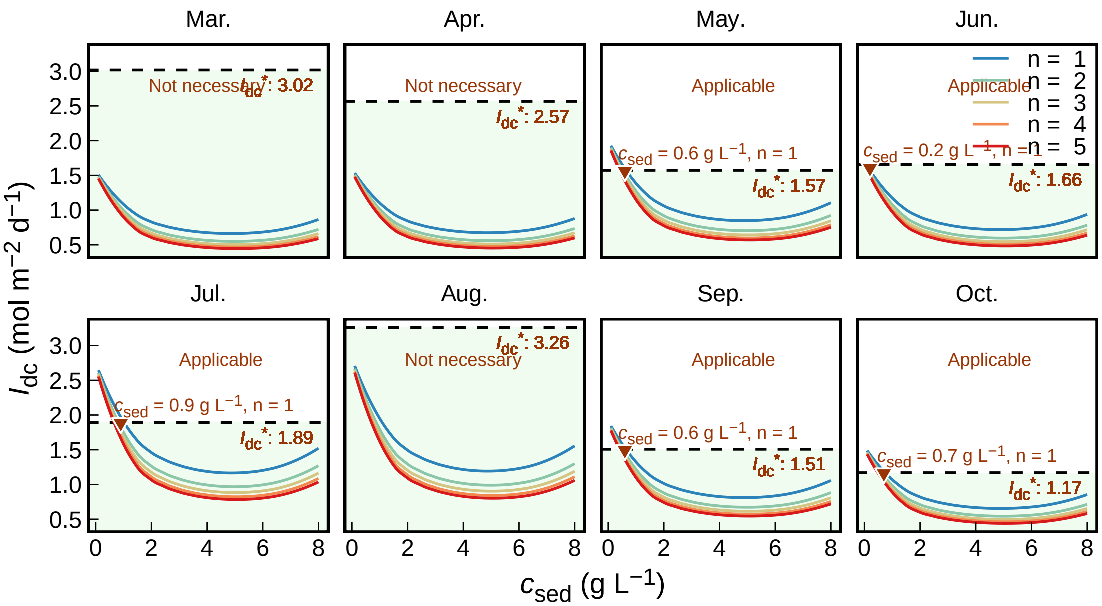

Fig. S31: Underwater light availability under varying sediment resuspension conditions in DTG reservoir (March - October).

No. 7 EJL Reservoir

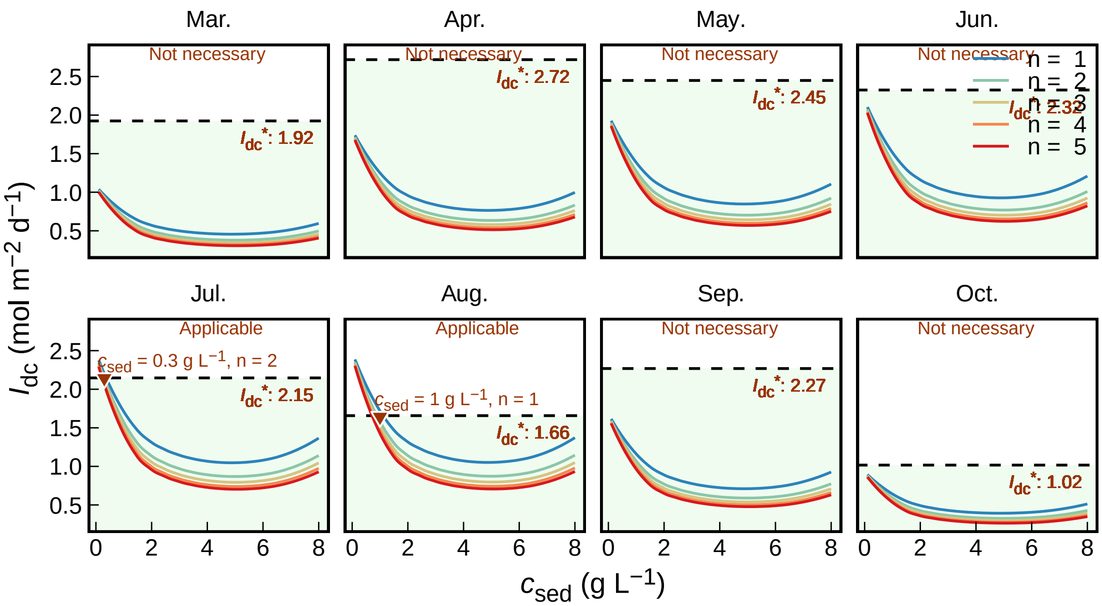

Fig. S32: Underwater light availability under varying sediment resuspension conditions in EJL reservoir (March - October).

No. 8 FH Reservoir

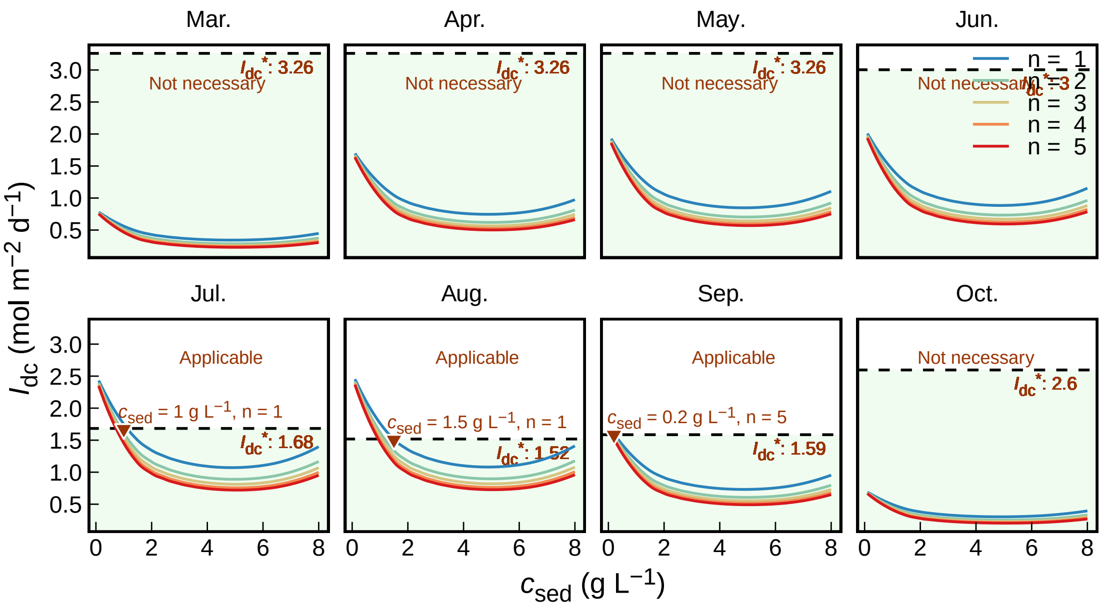

Fig. S33: Underwater light availability under varying sediment resuspension conditions in FH reservoir (March - October).

No. 9 FS Reservoir

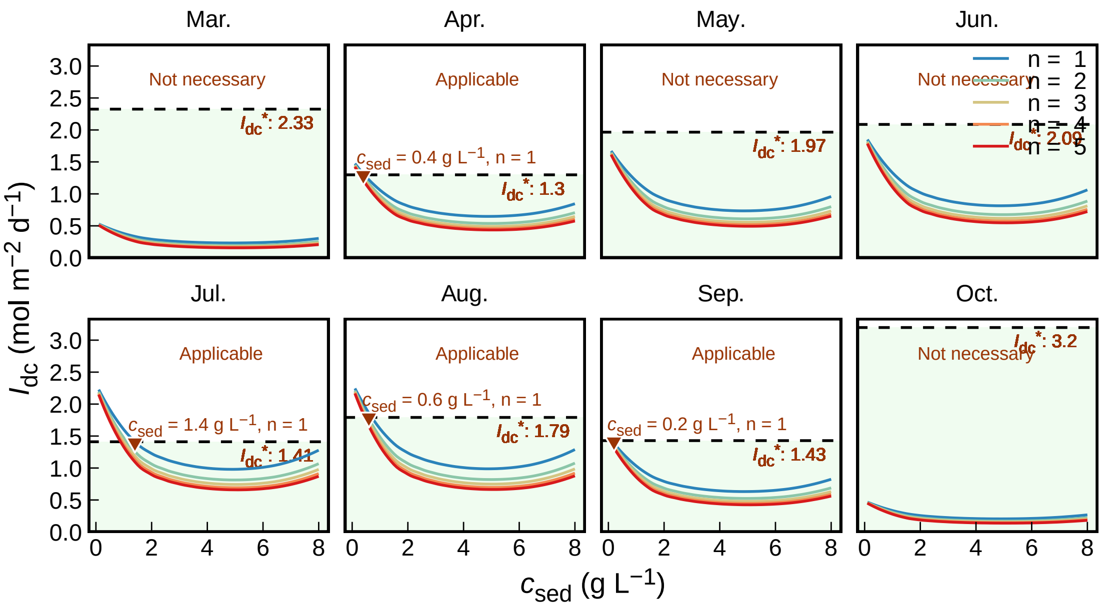

Fig. S34: Underwater light availability under varying sediment resuspension conditions in FS reservoir (March - October).

No. 10 GXZ Reservoir

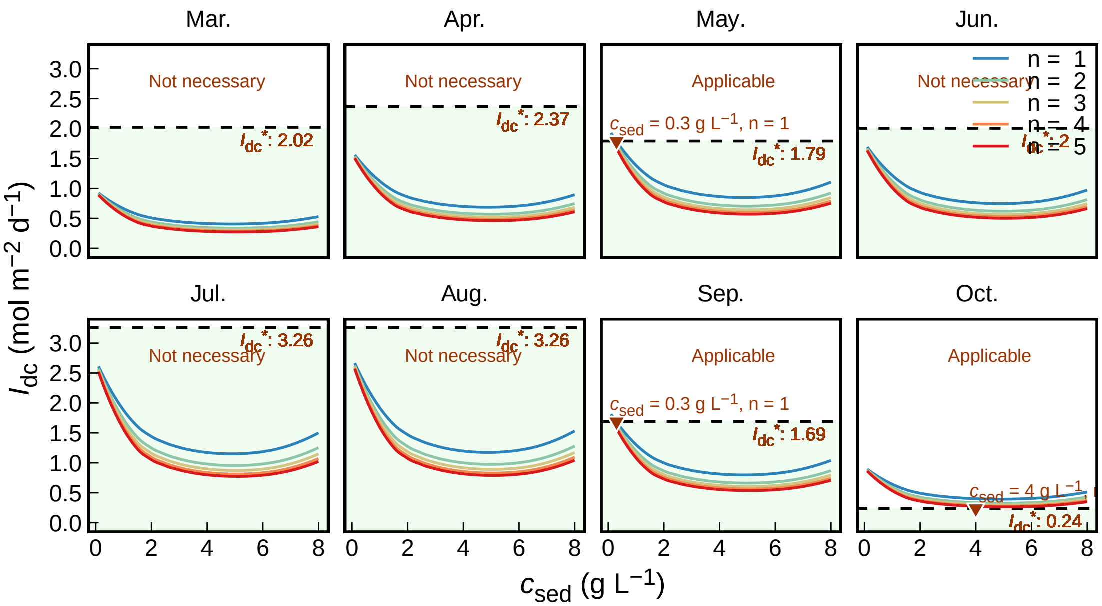

Fig. S35: Underwater light availability under varying sediment resuspension conditions in GXZ reservoir (March - October).

No. 11 HCG Reservoir

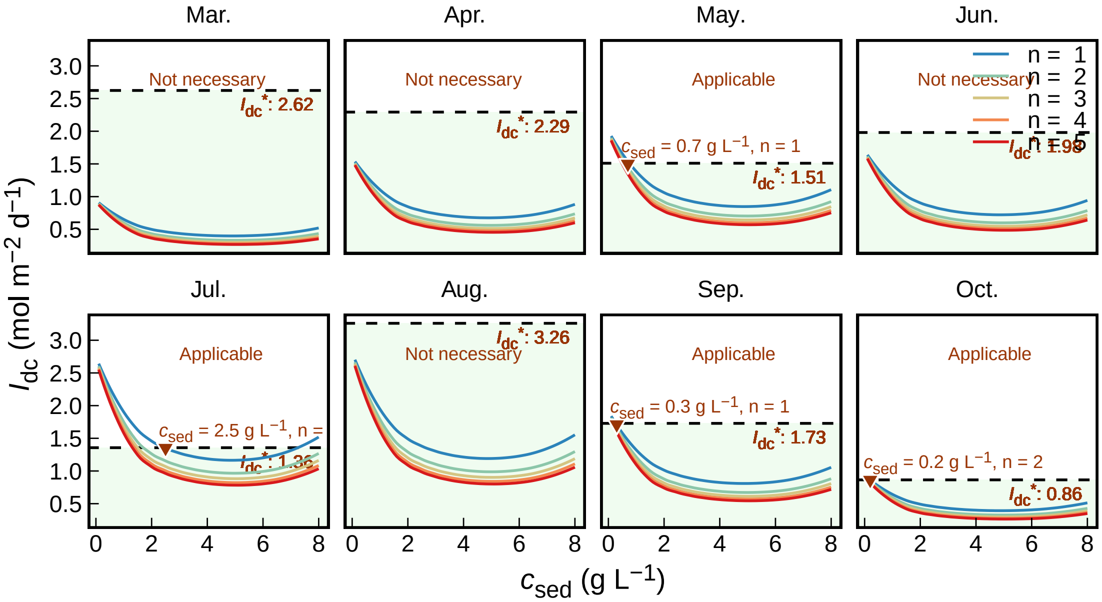

Fig. S36: Underwater light availability under varying sediment resuspension conditions in HCG reservoir (March - October).

No. 12 HJ Reservoir

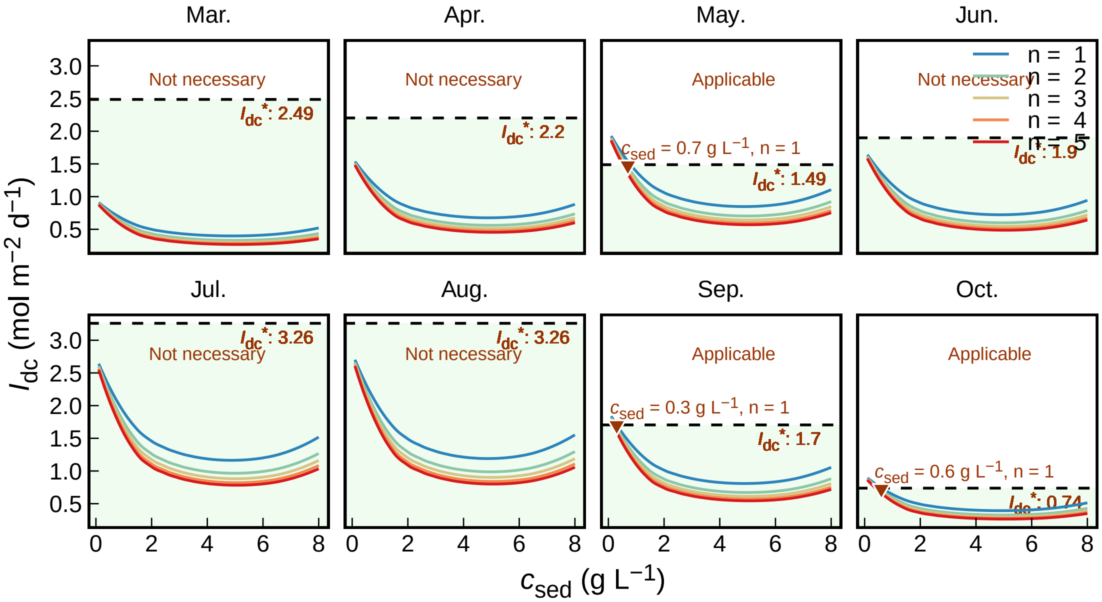

Fig. S37: Underwater light availability under varying sediment resuspension conditions in HJ reservoir (March - October).

No. 13 HK Reservoir

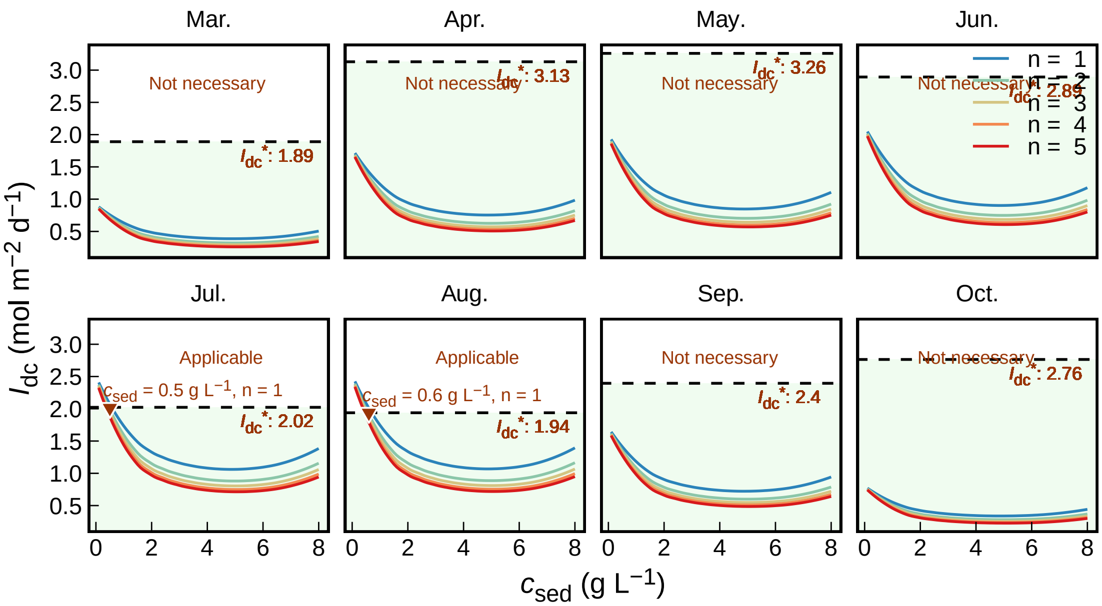

Fig. S38: Underwater light availability under varying sediment resuspension conditions in HK reservoir (March - October).

No. 14 HM Reservoir

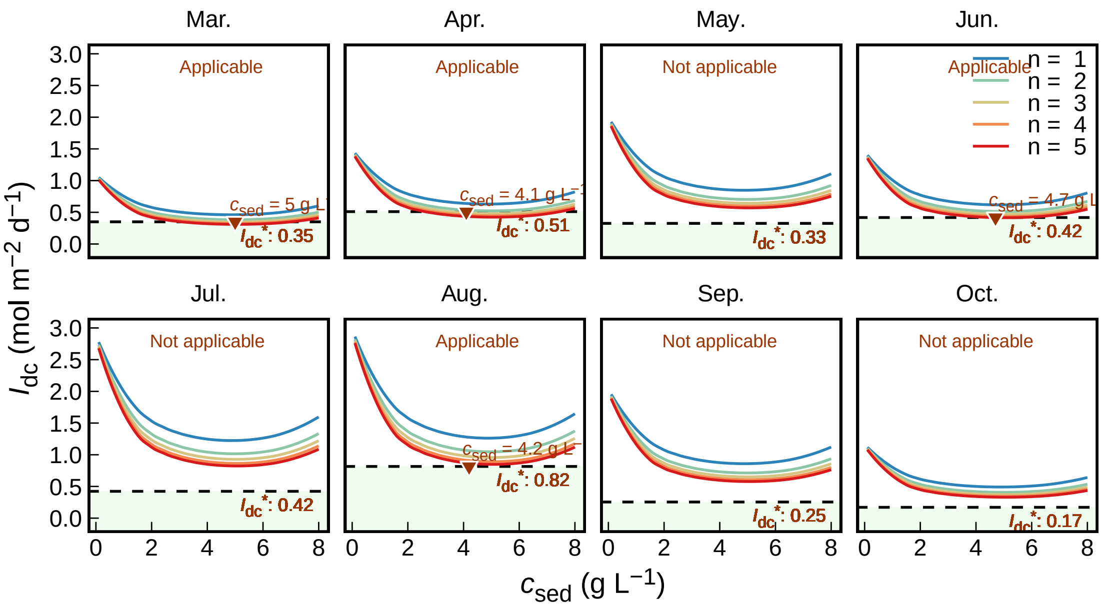

Fig. S39: Underwater light availability under varying sediment resuspension conditions in HM reservoir (March - October).

No. 15 HP Reservoir

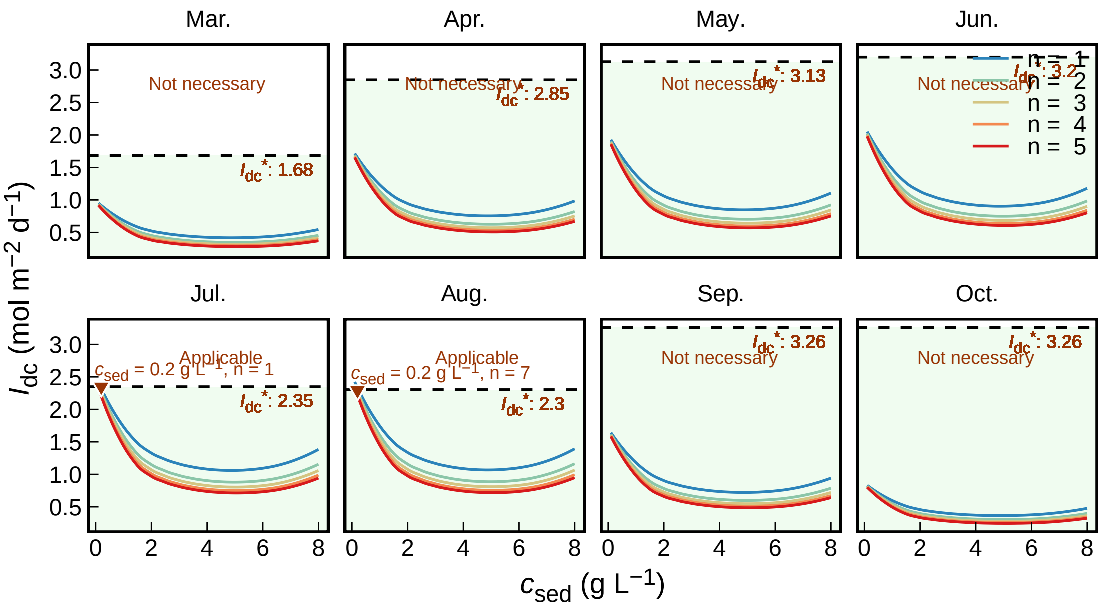

Fig. S40: Underwater light availability under varying sediment resuspension conditions in HP reservoir (March - October).

No. 16 HS Reservoir

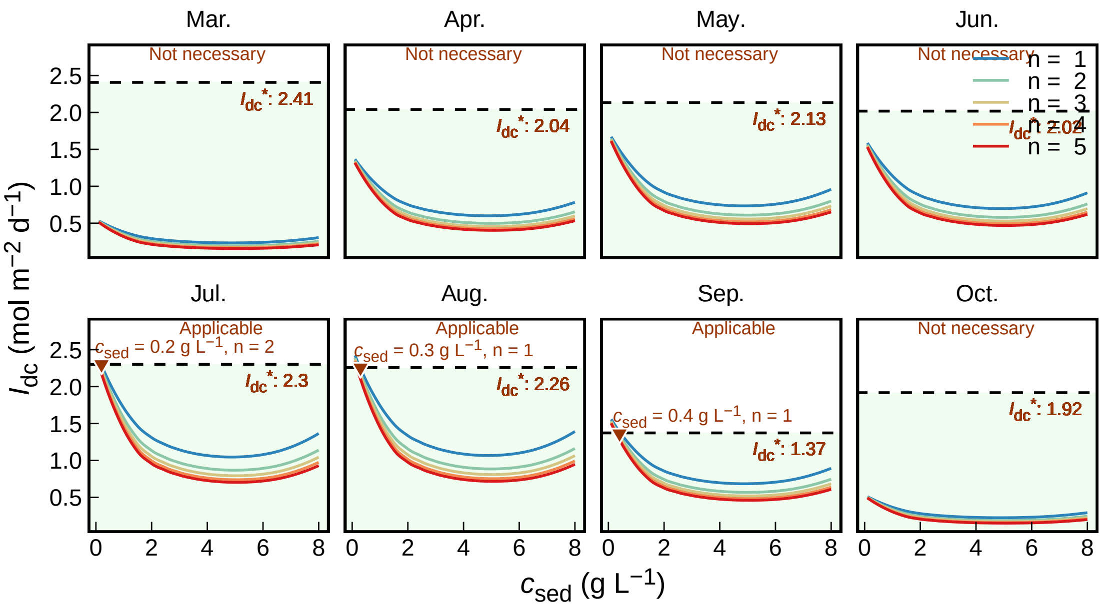

Fig. S41: Underwater light availability under varying sediment resuspension conditions in HS reservoir (March - October).

No. 17 HX Reservoir

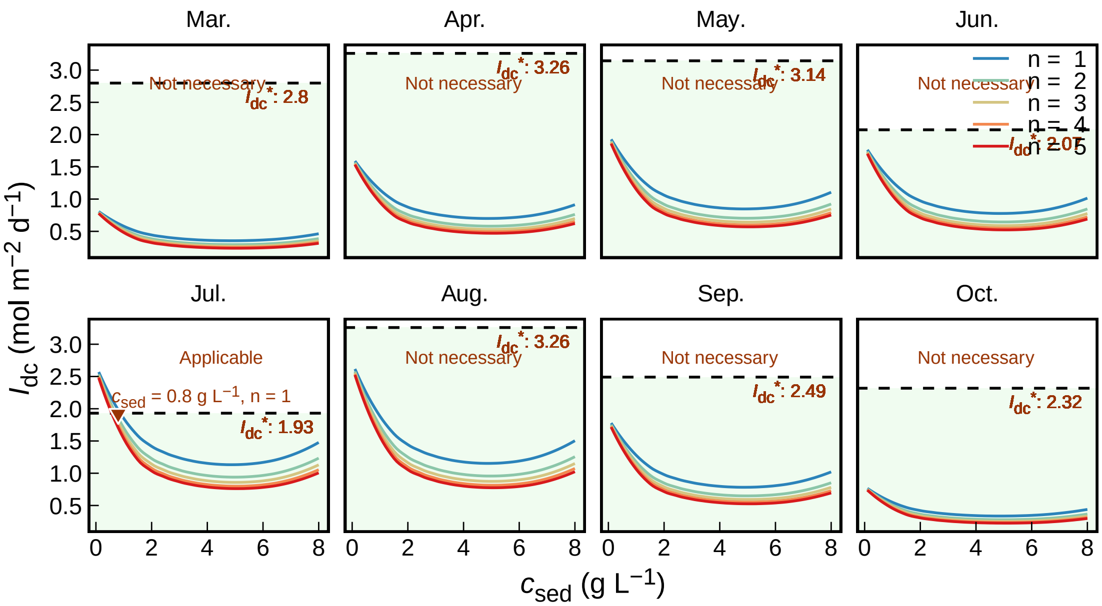

Fig. S42: Underwater light availability under varying sediment resuspension conditions in HX reservoir (March - October).

No. 18 HXH Reservoir

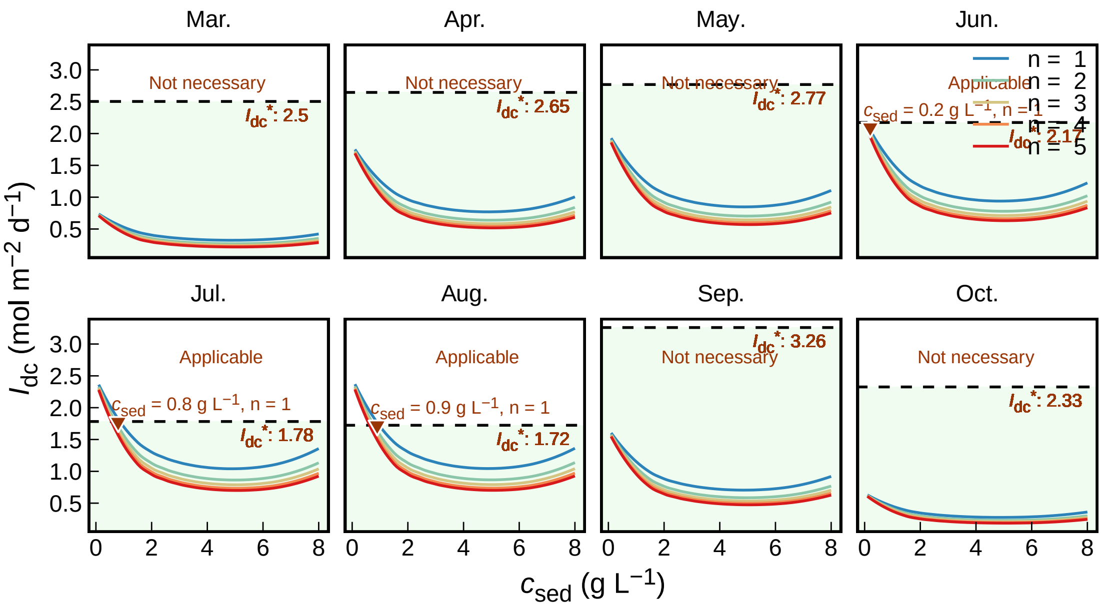

Fig. S43: Underwater light availability under varying sediment resuspension conditions in HXH reservoir (March - October).

No. 19 LH Reservoir

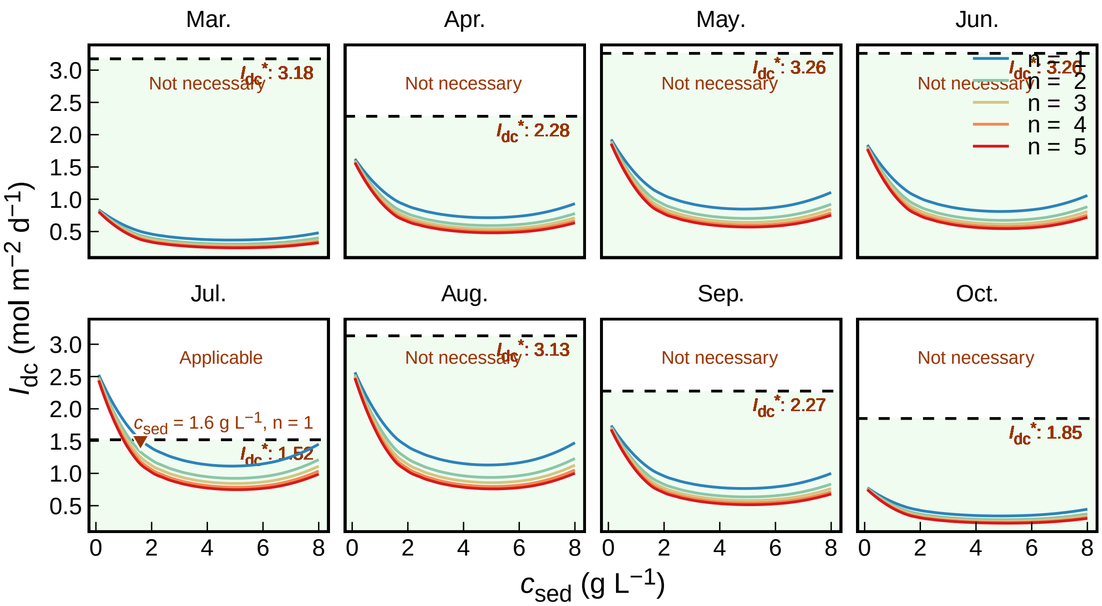

Fig. S44: Underwater light availability under varying sediment resuspension conditions in LH reservoir (March - October).

No. 20 LHT Reservoir

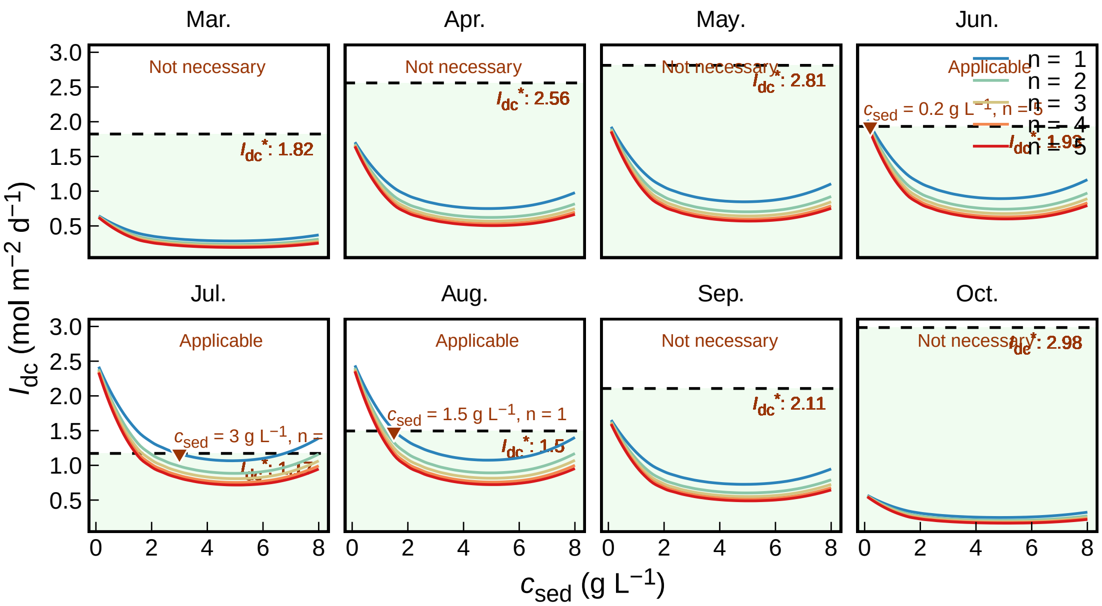

Fig. S45: Underwater light availability under varying sediment resuspension conditions in LHT reservoir (March - October).

No. 21 LSK Reservoir

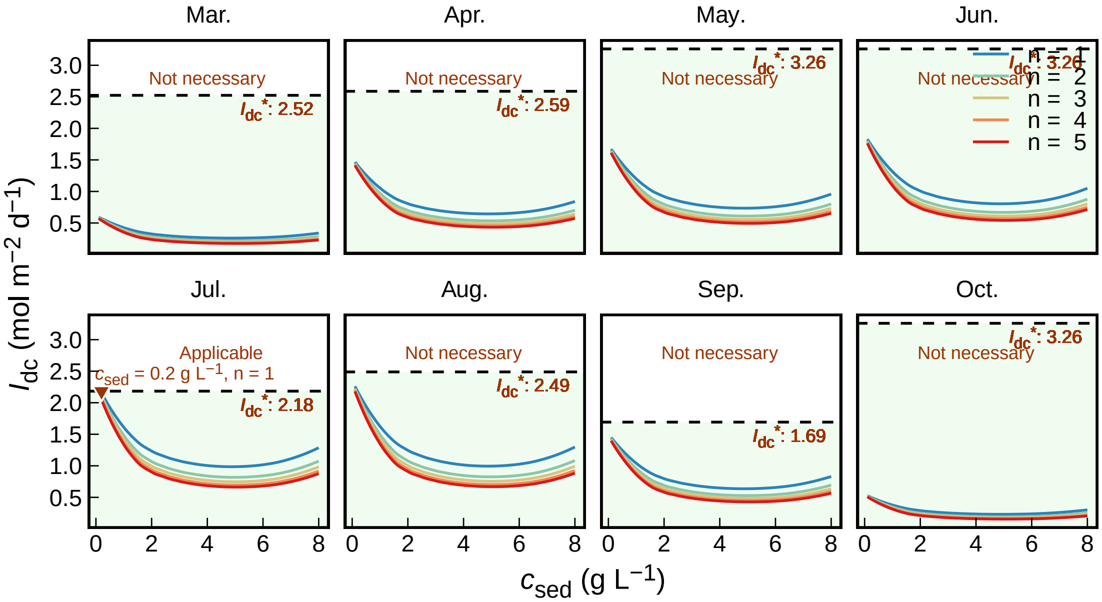

Fig. S46: Underwater light availability under varying sediment resuspension conditions in LSK reservoir (March - October).

No. 22 LY Reservoir

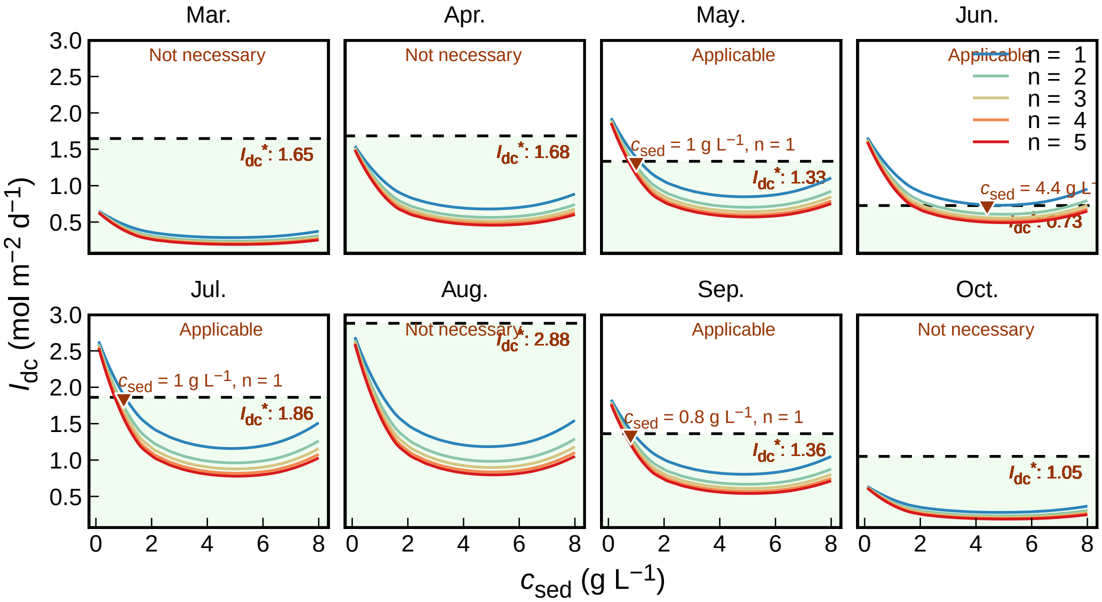

Fig. S47: Underwater light availability under varying sediment resuspension conditions in LY reservoir (March - October).

No. 23 MH Reservoir

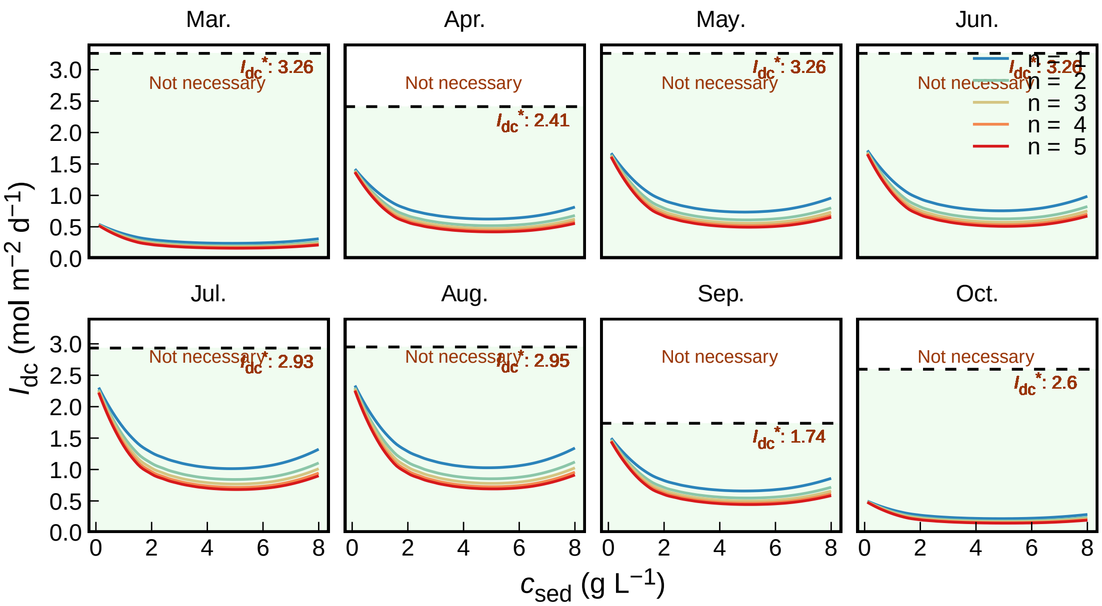

Fig. S48: Underwater light availability under varying sediment resuspension conditions in MH reservoir (March - October).

No. 24 MX Reservoir

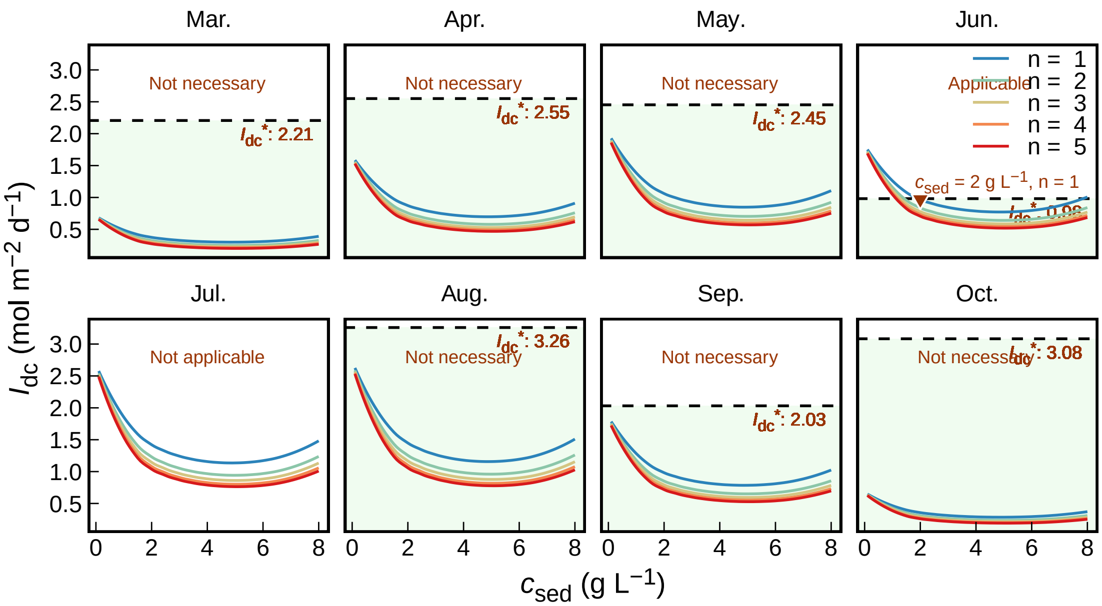

Fig. S49: Underwater light availability under varying sediment resuspension conditions in MX reservoir (March - October).

No. 25 NJ Reservoir

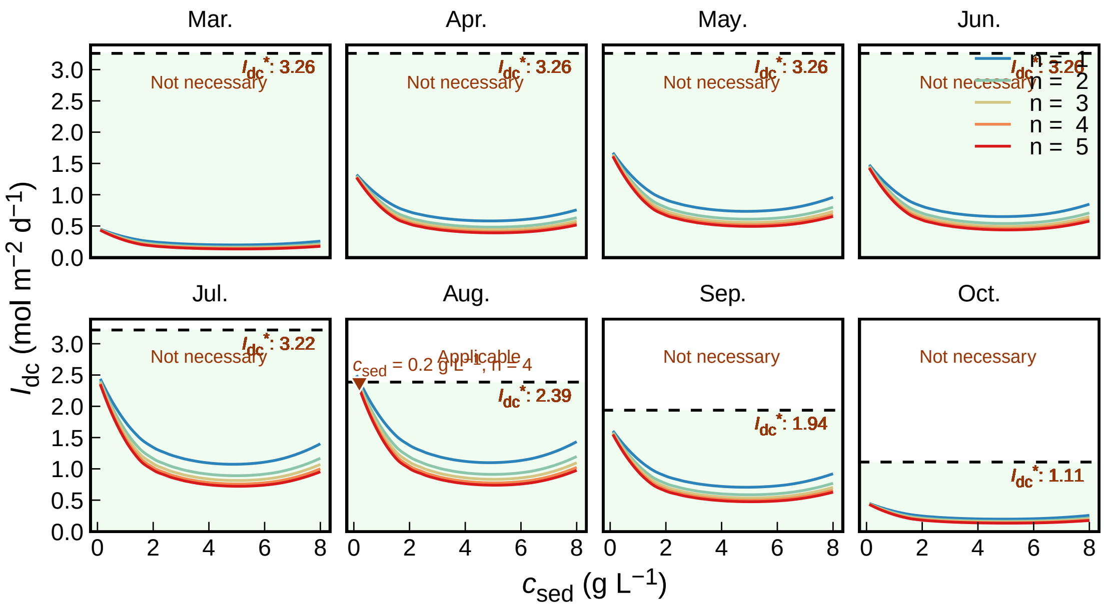

Fig. S50: Underwater light availability under varying sediment resuspension conditions in NJ reservoir (March - October).

No. 26 SA Reservoir

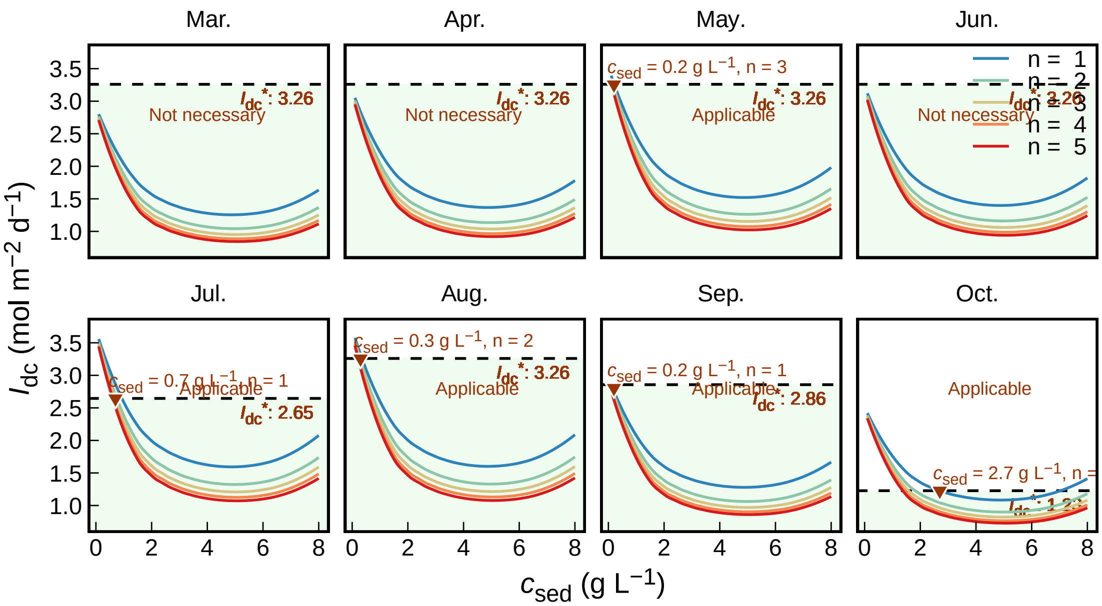

Fig. S51: Underwater light availability under varying sediment resuspension conditions in SA reservoir (March - October).

No. 27 SLH Reservoir

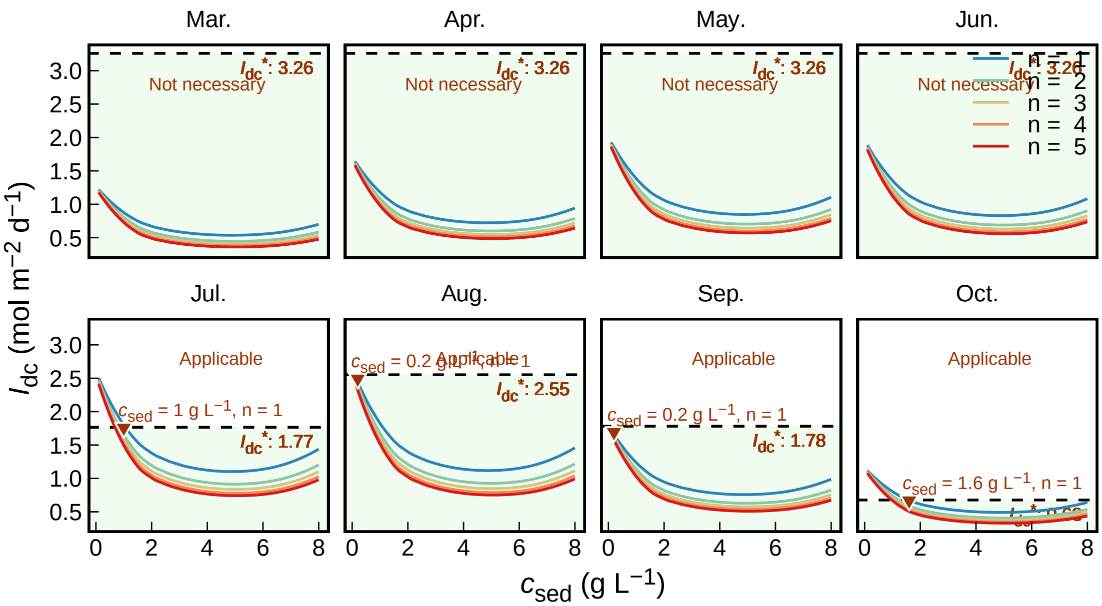

Fig. S52: Underwater light availability under varying sediment resuspension conditions in SLH reservoir (March - October).

No. 28 SLK Reservoir

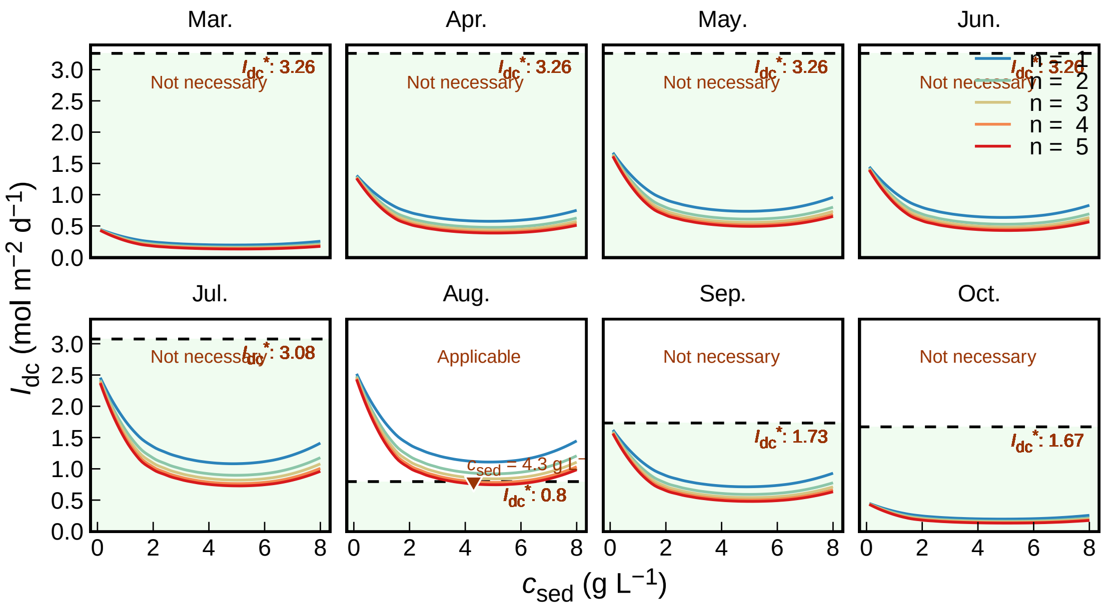

Fig. S53: Underwater light availability under varying sediment resuspension conditions in SLK reservoir (March - October).

No. 29 SMH Reservoir

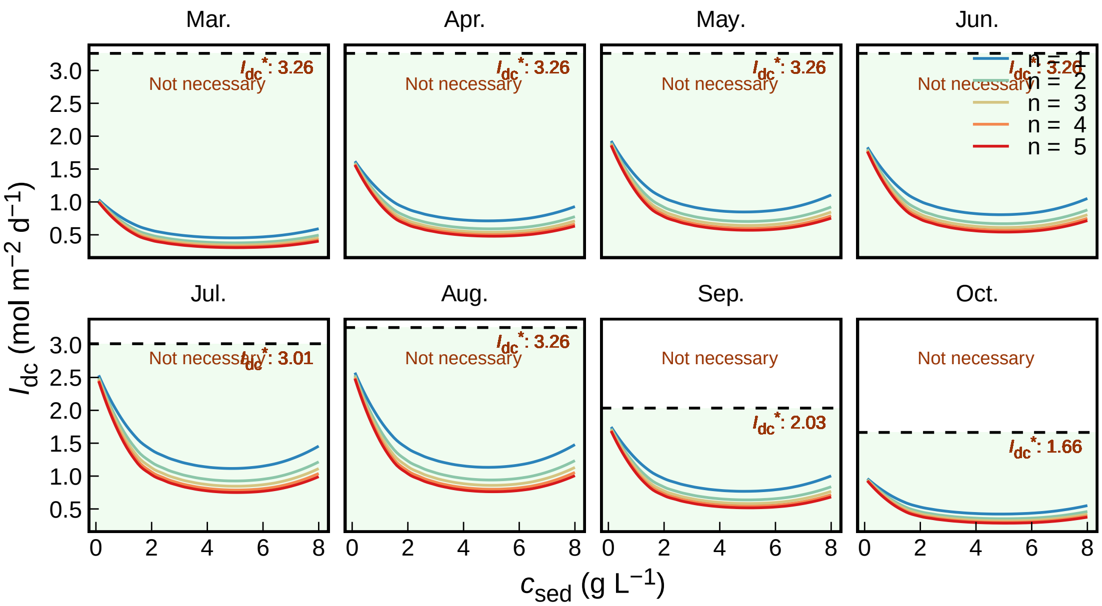

Fig. S54: Underwater light availability under varying sediment resuspension conditions in SMH reservoir (March - October).

No. 30 SXK Reservoir

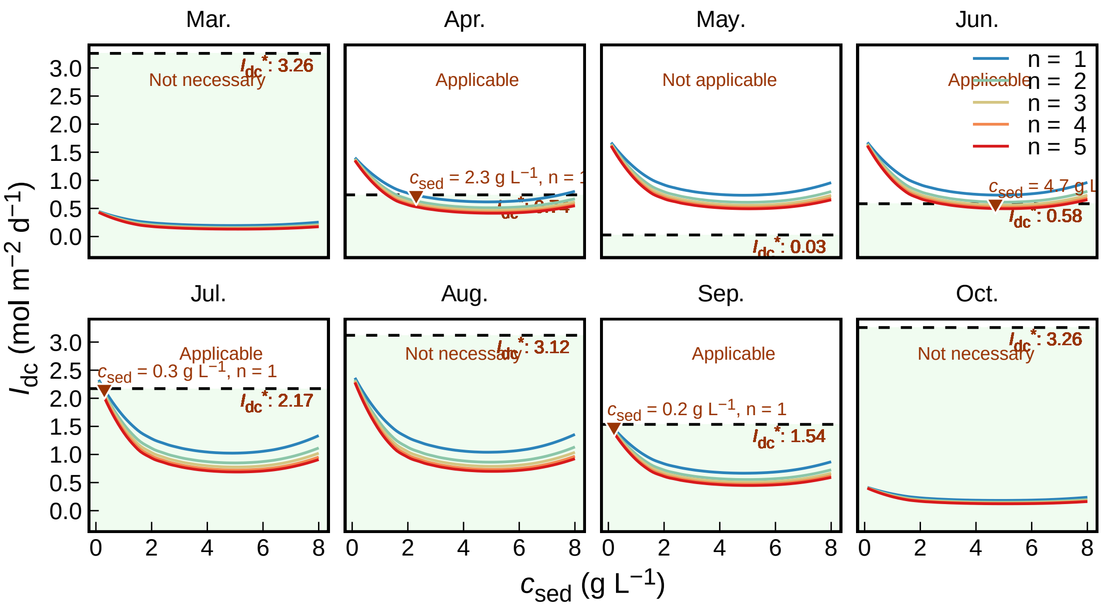

Fig. S55: Underwater light availability under varying sediment resuspension conditions in SXK reservoir (March - October).

No. 31 SXP Reservoir

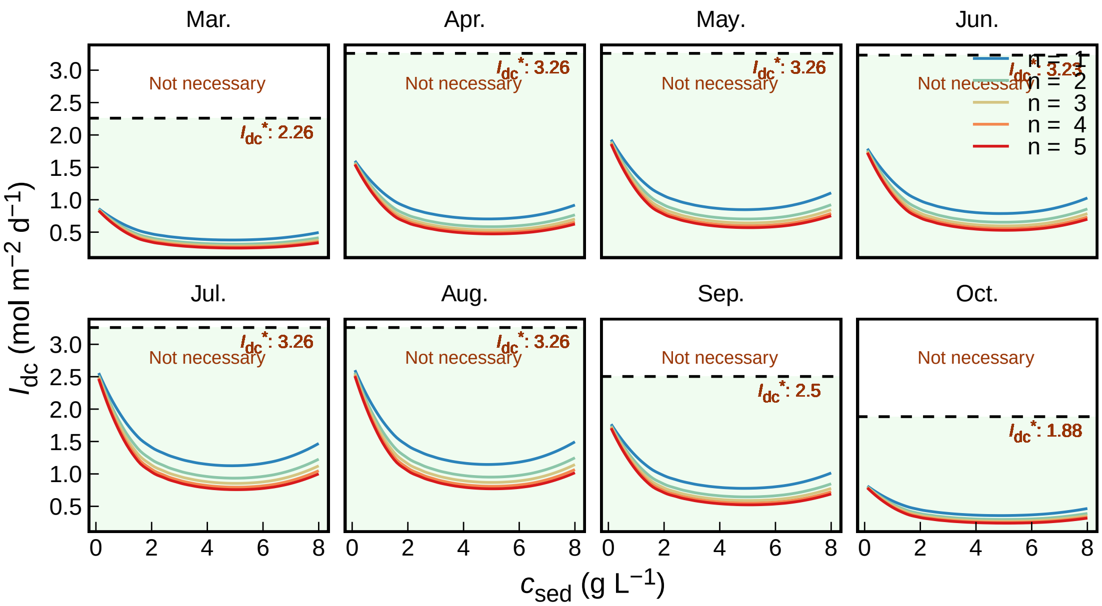

Fig. S56: Underwater light availability under varying sediment resuspension conditions in SXP reservoir (March - October).

No. 32 SZ Reservoir

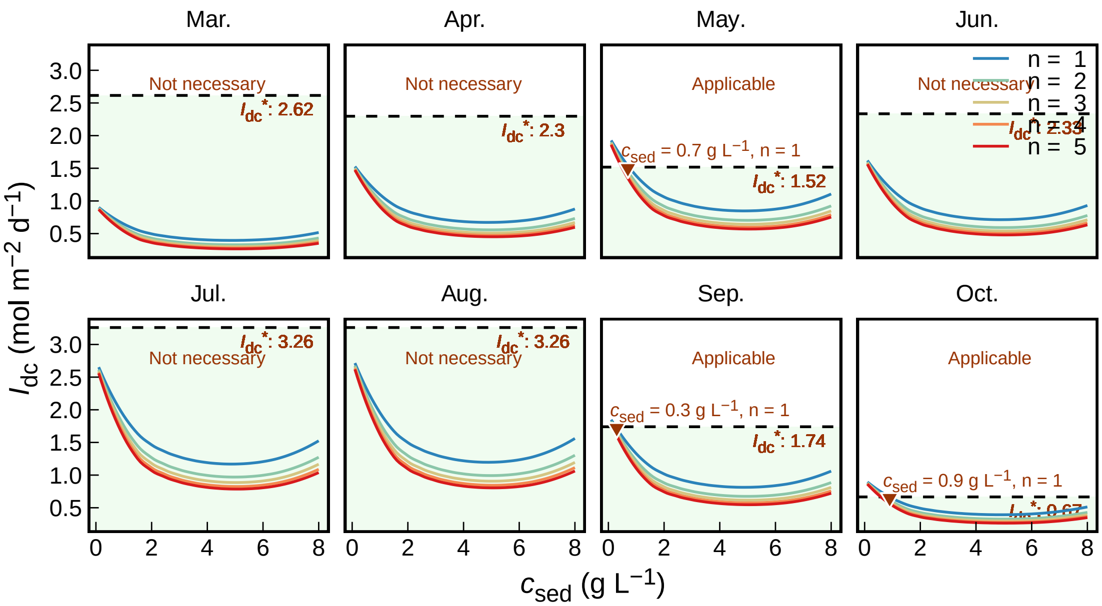

Fig. S57: Underwater light availability under varying sediment resuspension conditions in SZ reservoir (March - October).

No. 33 TX Reservoir

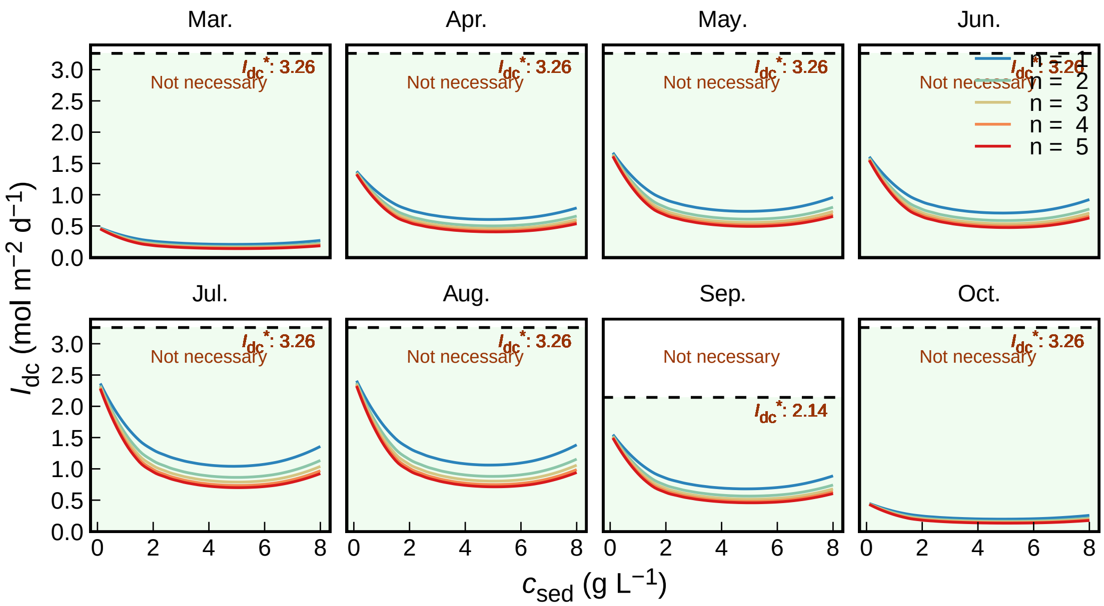

Fig. S58: Underwater light availability under varying sediment resuspension conditions in TX reservoir (March - October).

No. 34 TZG Reservoir

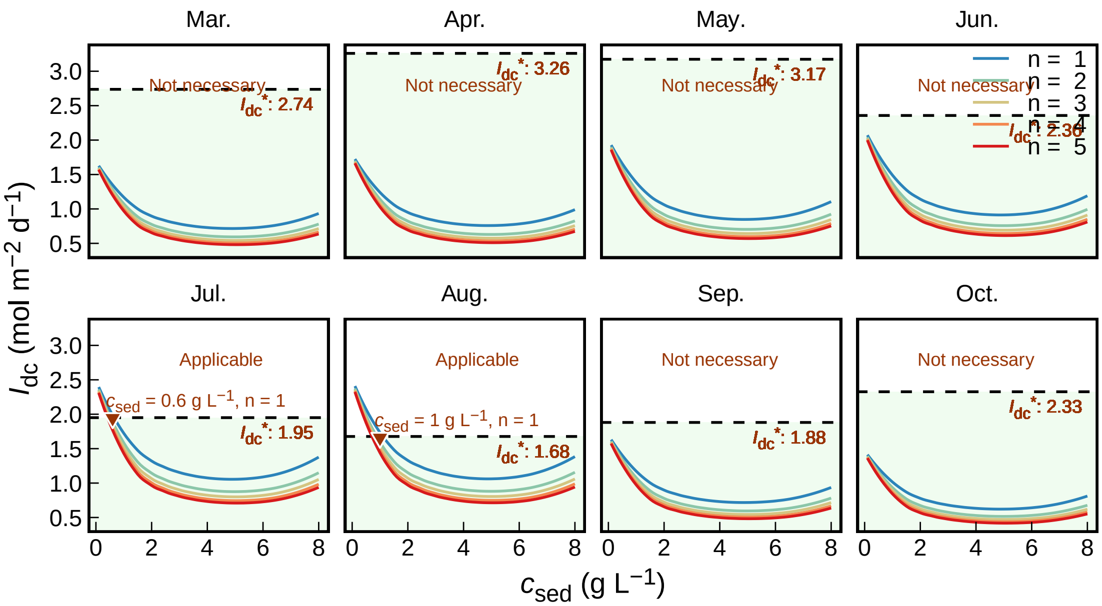

Fig. S59: Underwater light availability under varying sediment resuspension conditions in TZG reservoir (March - October).

No. 35 XK Reservoir

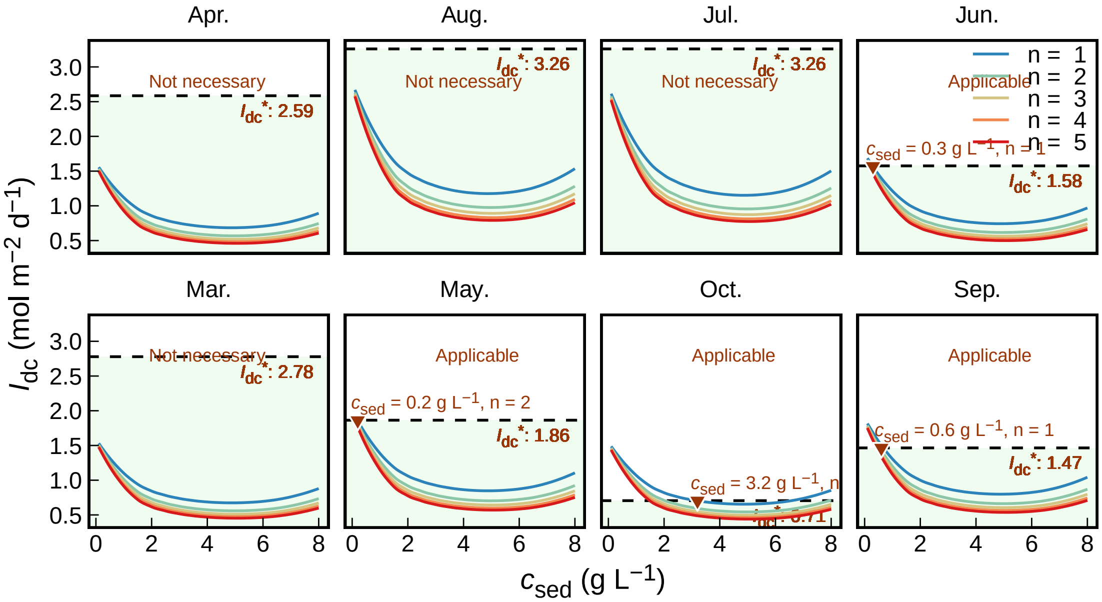

Fig. S60: Underwater light availability under varying sediment resuspension conditions in XK reservoir (March - October).

No. 36 XLA Reservoir

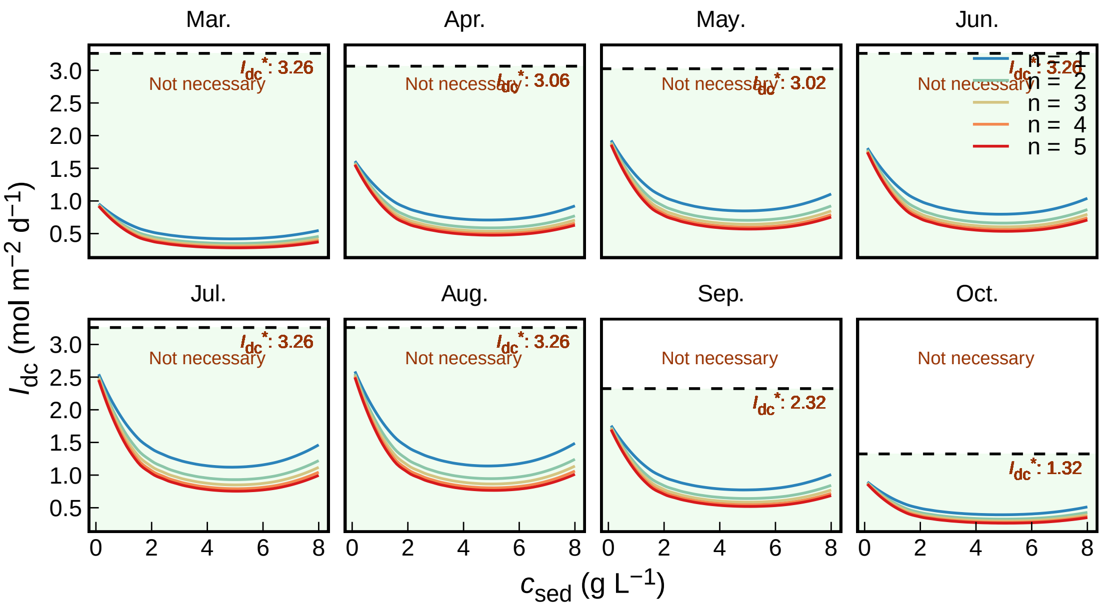

Fig. S61: Underwater light availability under varying sediment resuspension conditions in XLA reservoir (March - October).

No. 37 XXN Reservoir

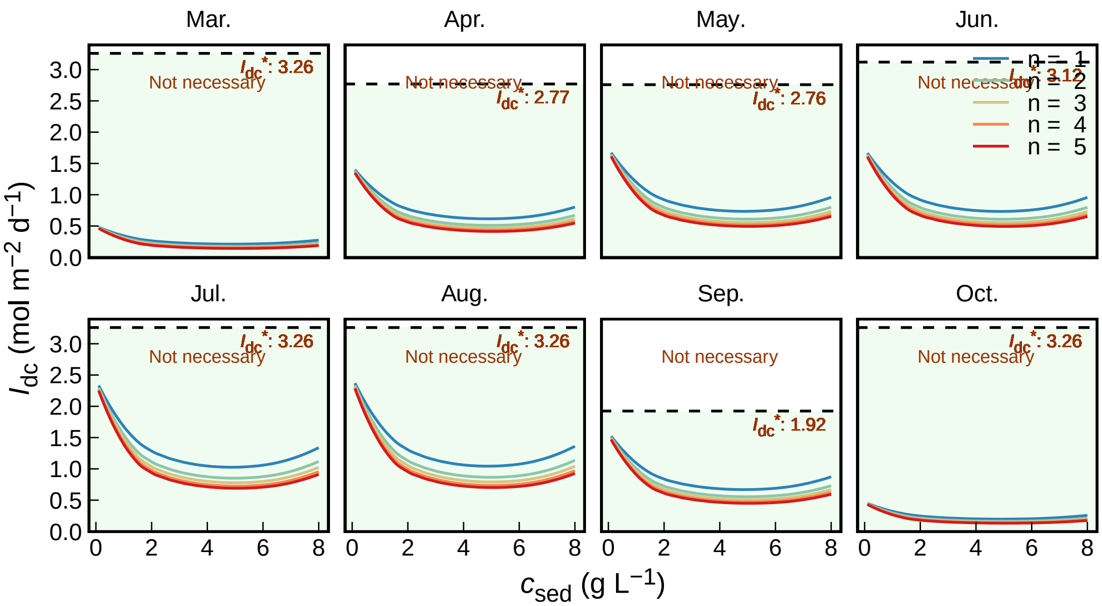

Fig. S62: Underwater light availability under varying sediment resuspension conditions in XXN reservoir (March - October).

No. 38 YML Reservoir

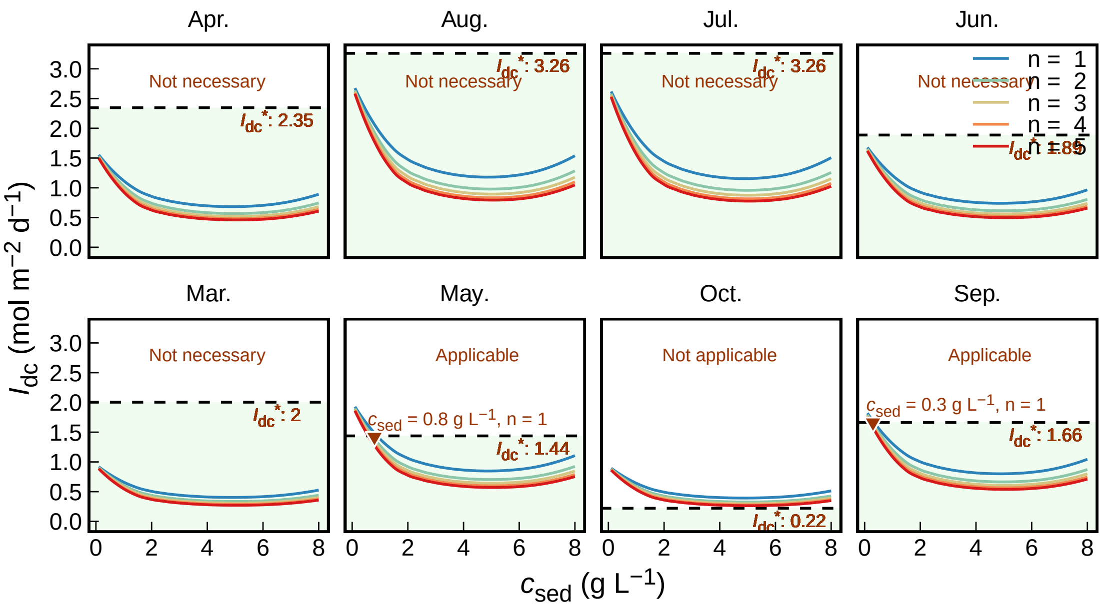

Fig. S63: Underwater light availability under varying sediment resuspension conditions in YML reservoir (March - October).

No. 39 ZGZ Reservoir

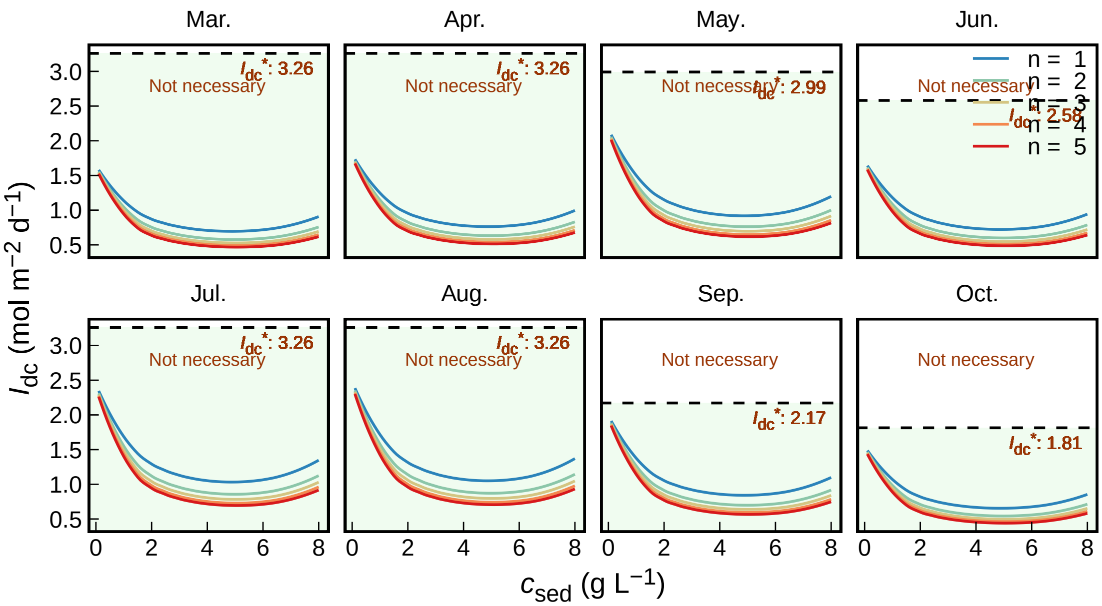

Fig. S64: Underwater light availability under varying sediment resuspension conditions in ZGZ reservoir (March - October).

No. 40 ZX Reservoir

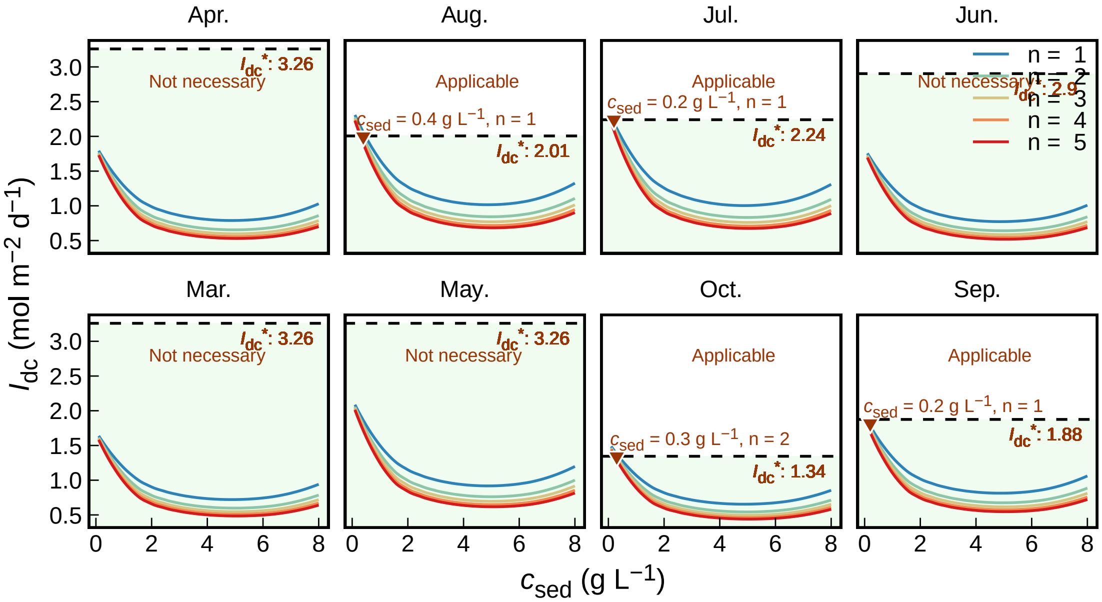

Fig. S65: Underwater light availability under varying sediment resuspension conditions in ZX reservoir (March - October).

References

Fang, J., Li, Y., Su, M., Cao, T., Sun, X., Ai, Y., Qin, J., Yu, J., Yang, M., 2024. Mitigating harmful cyanobacterial blooms in drinking water reservoirs through in-situ sediment resuspension. Water Research 267, 122509. https://doi.org/10.1016/j.watres.2024.122509

He, Q., Liu, Z., Li, M., 2024. Effects of aeration induced turbulence on colonial morphology and microcystin release of the bloom-forming cyanoabcterium microcystis. Journal of Oceanology and Limnology 42, 1827–1838. https://doi.org/10.1007/s00343-024-4096-7

Kong, Y., Peng, Y., Zhang, Z., Zhang, M., Zhou, Y., Duan, Z., 2019. Removal of *Microcystis aeruginosa* by ultrasound: Inactivation mechanism and release of algal organic matter. Ultrasonics Sonochemistry 56, 447–457. https://doi.org/10.1016/j.ultsonch.2019.04.017

Lee, K., Chantrasakdakul, P., Kim, D., Kong, M., Park, K.Y., 2014. Ultrasound pretreatment of filamentous algal biomass for enhanced biogas production. Waste Management 34, 1035–1040. https://doi.org/10.1016/j.wasman.2013.10.012

Li, H., Pan, G., 2015. Simultaneous removal of harmful algal blooms and microcystins using microorganism- and chitosan-modified local soil. Environmental Science & Technology 49, 6249–6256. https://doi.org/10.1021/acs.est.5b00840

Liu, H., Chen, S., Zhang, H., Wang, N., Ma, B., Liu, X., Niu, L., Yang, F., Xu, Y., Zhang, X., 2023. Effects of copper sulfate algaecide on the cell growth, physiological characteristics, the metabolic activity of *Microcystis aeruginosa* and raw water application. Journal of Hazardous Materials 445, 130604. https://doi.org/10.1016/j.jhazmat.2022.130604

Su, M., Li, W., Fang, J., Cao, T., Ai, Y., Lü, C., Zhao, J., Yang, Z., Yang, M., 2025. Effects of oxygenation resuspension on DOM composition and its role in reducing dissolved manganese in drinking water reservoirs. Environmental Science & Technology. https://doi.org/10.1021/acs.est.5c00235

Tsai, K.-P., 2016. Management of target algae by using copper-based algaecides: Effects of algal cell density and sensitivity to copper. Water, Air, & Soil Pollution 227. https://doi.org/10.1007/s11270-016-2926-8

Xu, H., Pang, Y., Li, Y., Zhang, S., Pei, H., 2021. Using sodium percarbonate to suppress vertically distributed filamentous cyanobacteria while maintaining the stability of microeukaryotic communities in drinking water reservoirs. Water Research 197, 117111. https://doi.org/10.1016/j.watres.2021.117111

Xu, H., Yang, A., Li, Z., Wang, W., Wang, X., Pei, H., 2024. Permanganate-enhanced coagulation for benthic filamentous *Pseudanabaena* sp. Removal: Control disinfection by-products during subsequent chlorination and prevent regrowth of algal cells in sludge. Journal of Water Process Engineering 64, 105730. https://doi.org/10.1016/j.jwpe.2024.105730